AGU PUBLICATIONS

JGR

Journal of Geophysical Research: Earth Surface

RESEARCH ARTICLE

10.1002/2015JF003445

Key Points:
- Accelerated tidal network ontogeny with increasing sediment supply
- Ecogeomorphic feedbacks enhanced for high biomass density at low marsh elevations
- Inheritance of tidal channel features from the initial tidal basin morphology

Supporting Information:
- Figures S1–S5

Correspondence to:
J.-P. Belliard,
jll.belliard@unitn.it

Citation:
Belliard, J.-P., M. Toffolon, L. Carniello, and A. D'Alpaos (2015), An ecogeomorphic model of tidal channel initiation and elaboration in progressive marsh accretional contexts, *J. Geophys. Res. Earth Surf.*, *120*, 1040–1064, doi:10.1002/2015JF003445.

Received 13 JAN 2015
Accepted 18 MAY 2015
Accepted article online 26 MAY 2015
Published online 24 JUN 2015

©2015. American Geophysical Union. All Rights Reserved.

An ecogeomorphic model of tidal channel initiation and elaboration in progressive marsh accretional contexts

J.-P. Belliard[1,2], M. Toffolon[1], L. Carniello[3], and A. D'Alpaos[4]

[1]Department of Civil, Environmental and Mechanical Engineering, University of Trento, Trento, Italy, [2]School of Geography, Queen Mary, University of London, London, UK, [3]Department of Civil, Environmental and Architectural Engineering, University of Padova, Padova, Italy, [4]Department of Geosciences, University of Padova, Padova, Italy

Abstract The formation and evolution of tidal networks have been described through various theories which mostly assume that tidal network development results from erosional processes, therefore emphasizing the chief role of external forcing triggering channel net erosion such as tidal currents. In contrast, in the present contribution we explore the influence of sediment supply in governing tidal channel initiation and further elaboration using an ecogeomorphic modeling framework. This deliberate choice of environmental conditions allows for the investigation of tidal network growth and development in different sedimentary contexts and provides evidences for the occurrence of both erosional and depositional channel-forming processes. Results show that these two mechanisms in reality coexist but act at different time scales: channel initiation stems from erosional processes, while channel elaboration mostly results from depositional processes. Furthermore, analyses suggest that tidal network ontogeny is accelerated as the marsh accretional activity increases, revealing the high magnitude and prevalence of the depositional processes in governing the morphodynamic evolution of the tidal network. On a second stage, we analyze the role of different initial topographic configurations in driving the development of tidal networks. Results point out an increase in network complexity over highly perturbed initial topographic surfaces, highlighting the legacy of initial conditions on channel morphological properties. Lastly, the consideration that landscape evolution depends significantly on the parameterization of the vegetation biomass distribution suggests that the claim to use uncalibrated models for vegetation dynamics is still questionable when studying real cases.

1. Introduction

Looking over a tidal wetland, the existence of a network characterized by an intricate system of branching and blind-ended channels clearly stands out from the overall landscape. Its striking appearance reflects in reality the complex nonlinear dynamics governing its morphological development. The mechanisms that originate and develop tidal channels are indeed complex and not fully understood so that an actual lack of consensus exists within the scientific community regarding the providence of a clear and detailed description of tidal channel ontogeny [*Perillo*, 2009]. Improving our understanding of the chief channel-forming processes is yet essential due to the primary role of the tidal network in providing a broad range of ecosystem services within the tidal wetland [*Barbier et al.*, 2011].

Although tidal networks and their intrinsic channels have not been studied as deeply as their fluvial counterparts, this intriguing problem has become a subject of great scientific interest, especially over the last decades, and a large body of literature have consequently emerged describing tidal network formation and evolution [e.g., *Fagherazzi and Overeem*, 2007; *De Swart and Zimmerman*, 2009; *Fagherazzi et al.*, 2012; *Hughes*, 2012; *Coco et al.*, 2013].

The dominant paradigm for tidal channel initiation and early development can be attributed to channel incision. Fundamentally, tidal channels develop in particular physical features, usually mudflats and to a lesser extent sandflats. These landforms are characterized by topographic perturbations which concentrate the tidal sheet flow into local depressions, producing scours where the local shear stress exceeds a threshold value for erosion. The resulting incised patterns favor a further flux concentration due to their expanding cross-sectional areas associated with the decreasing flow resistance as the forming course deepens, triggering

higher bed shear stress [e.g., *Fagherazzi and Furbish*, 2001]. These concomitant actions of erosion and course deepening reveal the existence of a positive feedback mechanism between erosion and channel formation, defining the concept of headward erosion [e.g., *D'Alpaos et al.*, 2005].

The conceptual model of tidal channel initiation based on plant/flow interactions described by *Yapp et al.* [1917] complements this paradigm, where growing hummocks provide an additional factor driving flow concentration into preferential locations, thus favoring the appearance of drainage patterns during ebb tide which soon after starts cutting shallow winding channels.

However, a series of observations have called for alternative mechanisms to explain tidal channel formation. For instance, *Perillo et al.* [1996] proposed a conceptual model for tidal channel formation based on the interconnection of salt ponds as a result of the combined action of wind/wave erosion occurring in a salt marsh system in southern Argentina. Other channel-forming mechanisms, although peculiar to certain locations, reflect the notable role of the benthos in driving tidal channel initiation. Correspondingly, *Perillo and Iribarne* [2003a, 2003b] introduced a conceptual model following observations in the Bahía Blanca estuary, Argentina, where the development of highly excavated salt pans as a result of crab/plant interactions leads to the formation of channels mediated by tidal and groundwater actions. An analogous mechanism put forward by *Hughes et al.* [2009] explains the extension of tidal creeks in a salt marsh in South Carolina, USA, where intense crab-burrowing activity coupled with vegetation dieback produces depressions located at the creek head which become channelized eventually.

These conceptual models of tidal channel formation and initial development assume an erosive action of the various physical and biological processes involved in the morphodynamic evolution and are therefore referred to as erosional models.

On the contrary, *Hood* [2006] proposed a depositional model for tidal channel formation stemming from observations in the Skagit River Delta, Washington, USA. In this particular estuarine environment, the formation of tidal channels results from the deposition of sediments along the river course forming progressively marsh islands separated by river distributaries which are eventually blocked by more sediments to become blind tidal channels. This sequence of events reveals the presence of a series of morphological processes such as differential deposition, channel elongation, gradient reduction, and channel senescence, as being part of a global systemic depositional process of marsh progradation, and therefore defining a conceptual model of depositional tidal channel formation [*Hood*, 2006, 2010]. Examples of tidal channel formation through depositional processes were also noticed in other tidal landscape units under accretional activity [e.g., *Redfield*, 1972], suggesting that marsh progradation is a necessary condition for the development of depositional tidal channels.

Practically, this diversity of channel-forming processes is not reflected in mathematical models as, except for a few cases [e.g., *Kirwan and Murray*, 2007], they mostly assume an erosional channel formation, notably through the mechanism of headward growth. In this regard, several modeling studies have investigated the role of external forcings inducing channel net erosion such as tidal range [e.g., *Van Maanen et al.*, 2013a] and relative sea level rise [e.g., *D'Alpaos et al.*, 2007; *Van Maanen et al.*, 2013b]. However, despite its potential implication in the morphological development of tidal channels [*Hood*, 2006], the role of sediment supply has not been explored individually from a modeling perspective. Accordingly, we develop a modeling framework to investigate this control on tidal channel morphodynamics. On a second stage, the analysis is extended to the exploration of the role of the initial bathymetry in driving the dynamic response of the system, by considering random initial topographic perturbations with different scenarios of amplitudes and degrees of smoothness.

As tidal networks are tightly coupled with the tidal flat and salt marsh landforms onto which they develop, a holistic approach is adopted by simulating the coevolution of the marsh platform with the embedded tidal networks in analogy with *Kirwan and Murray* [2007]. However, doing so leads to a typical challenge regarding the inclusion of biotic processes and their related feedbacks with hydrodynamics and sediment transport. In the present case, a morphodynamic model built upon the work of *Defina* [2000] and later extended by *Carniello et al.* [2005, 2011, 2012] is adopted and is then coupled with the development of an ecological module simulating vegetation growth and the related ecogeomorphic processes. While the hydrodynamic and morphodynamic modules solve fast- and detailed-scale variables, the ecological module corresponds to a process-based model incorporating a simplified mathematical description of the vegetation dynamics which is based on long-term assumptions, therefore making the modeling framework a "hybrid" tool.

Through this modeling framework, our motivation is to bring further insights into the mechanisms governing the formation and evolution of tidal networks. Particularly, the emphasis is placed on the investigation of (i) how tidal networks form and evolve in different sedimentary contexts, (ii) how they form and evolve starting from different initial tidal flat bathymetric configurations, and (iii) how they respond to ecogeomorphic feedbacks involving different ecological scenarios and mathematical parameterizations.

2. The Modeling Framework

The evolution of the salt marsh landscape is studied on the basis of the ecomorphodynamic approach; i.e., the modeling framework considers interactions and feedbacks between processes (mainly tidal currents) and morphology, driven by sediment transport and mediated by vegetation growth through related ecogeomorphic processes. In the following we will describe these different constituents prior to discussing on the numerical setting.

2.1. Hydrodynamic and Morphodynamic Models

The mechanical interaction of tidal currents and waves with sediments is described on the basis of the two-dimensional (2-D) model originally developed by *Defina* [2000], with the inclusion of the WWTM (Wind Wave Tidal Model) and STABEM (Sediment Transport And Bed Evolution Model) modules developed by *Carniello et al.* [2005, 2011, 2012].

The hydrodynamic model was specifically designed to study very shallow tidal basins. Indeed, tidal landforms such as salt marshes and tidal flats present wide portions of the ground surface being subject to repetitive flooding and drying processes. To deal with flows in highly irregular topography, the usual shallow water equations are modified in order to account for partially wet domains: a phase-averaging procedure is first applied to the original Reynolds equations prior to integrating the resulting equations over the depth. We refer the reader to *Defina* [2000] for the complete derivation of the governing equations.

The morphodynamic model, which encompasses the coupled sediment transport and bed evolution modules, has been designed to simulate the resuspension, transport, and deposition of sediments by wind waves and tidal currents offering the possibility to include a two size-class mixture of sediments (cohesive and noncohesive). In the present study, we focus our attention on the evolution of tidal channels and salt marshes under progressive accretional activity which can characterize the innermost areas of tidal environments. For this reason, consistently with field observations, only one sedimentological class of cohesive material is considered and the wind wave effect is neglected in view of the highly limited fetch characterizing these areas. We invite the reader to refer to *Carniello et al.* [2012, 2014] for a full description of the morphodynamic module and its peculiarities.

The following 2-D advection-dispersion equation is used to describe the transport of cohesive sediments:

$$\frac{\partial (CY)}{\partial t} + \nabla \cdot (\mathbf{q}\, C) - \nabla \cdot (\mathbf{D} Y \nabla C) = Q_e - Q_d\,, \tag{1}$$

where $C(\mathbf{x}, t)$ is the depth-averaged volumetric sediment concentration, Y is the flow depth, t is time, $\mathbf{D}$ is the two-dimensional diffusion tensor, and Q_e and Q_d are the erosion and deposition fluxes, respectively. Moreover, $\mathbf{q} = \{uY, vY\}$ is the vector of depth-integrated phase-averaged velocities (discharge per unit width), with u and v the velocity components along the directions x and y, respectively. Equation (1) can be simplified by assuming that the dispersion is negligible compared to advection [*Pritchard and Hogg*, 2003].

The evolution of bed topography results from mass conservation which, considering a single size of sediment particles, reads

$$(1-p)\frac{\partial \zeta}{\partial t} = Q_d - Q_e \tag{2}$$

where ζ is the local bottom elevation and p is the bed porosity which is assumed constant in our analyses, thus neglecting compaction processes. Equation (2) stipulates that the morphological changes derive directly from the net balance between erosion, Q_e, and deposition, Q_d, rates.

In the absence of vegetation, the erosion flux Q_{e_0} can be expressed as

$$Q_{e_0} = M_m T, \tag{3}$$

where M_m is the entrainment coefficient for pure mud and

$$T = -1 + \left[1 + \left(\frac{\tau_g}{\tau_{cr,e}}\right)^2\right]^{1/2}, \quad (4)$$

is the transport parameter, τ_g is the bottom shear stress directly acting on the bed material, and $\tau_{cr,e}$ is the critical shear stress for erosion. Equation (4) slightly departs from the classic transport parameter formulation of *Van Rijn* [1984] by depicting a smooth transition between $T = 0$ and $T = (\tau_g - \tau_{cr,e})/\tau_{cr,e}$, which must be correctly reproduced in tidal environments where bed shear stress assumes values close to the critical shear stress and whose rationale is explained in *Carniello et al.* [2012]. The erosion flux Q_{e_0} can be also influenced in relation to some ecogeomorphic mechanisms coming into play as soon as vegetation starts colonizing portions of the tidal domain and will be reviewed in the next section.

The presence of vegetation can influence also the deposition flux Q_d, which is therefore made up of three contributions as follows:

$$Q_d = Q_{dt} + Q_{db} + Q_{ds} \quad (5)$$

where Q_{dt} is the rate of particle capture by plant stems, Q_{db} is the production of organic sediments due to the presence of vegetation, and Q_{ds} is the settling rate of inorganic sediments possibly enhanced due to plant drag. These ecosedimentary processes will be described in the following section. Obviously, if the marsh is not vegetated, both Q_{dt} and Q_{db} vanish, whereas Q_{ds} only depends on physical processes (settling of sediments) evaluated by the formula proposed by *Krone* [1962]:

$$Q_{ds} = w_s C \max\left[0; \left(1 - \frac{\tau_g}{\tau_{cr,d}}\right)\right] \quad (6)$$

where w_s is the particle settling velocity and $\tau_{cr,d}$ is a critical shear stress for deposition.

2.2. The Ecological Module

The halophytic vegetation colonizing the marsh platform dissected by tidal networks is often termed as an "ecosystem engineer" [*Jones et al.*, 1994], capable of tuning the landscape topography to elevation ranges offering more favorable conditions for its growth [e.g., *Marani et al.*, 2013]. This contribution to the overall landscape morphological evolution is possible through a range of ecogeomorphic processes. Vegetation productivity contributes to sedimentation on the marsh platform by means of the three processes reported in equation (5): the capture of sediments by plant stems through the canopy Q_{dt}, the production of organic sediments Q_{db}, and the enhanced settling of inorganic sediments Q_{ds} due to plant drag leading to a reduction of the turbulence and velocity through the canopy [e.g., *Mudd et al.*, 2010]. Such mechanisms account for the coupling between biotic factors (e.g., plants) and physical processes and depend on vegetation characteristics, particularly on plant biomass that becomes necessary to evaluate.

In a given estuary with relatively constant tidal amplitude, temperature, and sediment supply, marsh elevation becomes the dominant factor in determining plant biomass [*Morris et al.*, 2002]. We therefore describe the spatial distribution of the biomass density B as a function of the local bottom elevation ζ:

$$B(\zeta) = b(\zeta) B_{max}, \quad (7)$$

where B_{max} is the maximum biomass density and $b(\zeta) \in (0, 1)$ represents the distribution of the dimensionless biomass density within the tidal frame.

The structure of equation (7) implies that biomass adapts instantaneously to elevation change. Although this assumption is not strictly valid (e.g., because of the seasonal variations) on a short time scale, it holds, however, over medium-to-long temporal scales, when the analysis does not aim to reproduce the actual sequence of the vegetation colonization but only the net results over a few years. As we will discuss later, this assumption is also consistent with the use of a relatively large morphological factor for accelerating the morphodynamic simulations. Nonetheless, this formulation provides a simple quantitative means for the representation of the well-documented feedback between salt marsh ecology (marsh vegetation) and geomorphology (marsh elevation) [*Marani et al.*, 2007, 2010].

Different parameterizations can be adopted for the biomass-elevation relationship $b(\zeta)$ in equation (7). In particular, we consider two cases: a continuous relationship modified after *Marani et al.* [2013] and a simplified discontinuous linear relationship reported in *D'Alpaos et al.* [2007]. Referring, for sake of simplicity, to the dimensionless biomass density $b(\zeta)$, we recast the *Marani et al.* [2013] continuous formulation as $b(\zeta) = f(\zeta)/f_{max}$, where

$$f(\zeta) = \frac{2}{\exp\left(\lambda_1\left(\zeta - \zeta_0\right)\right) + \exp\left(-\lambda_2\left(\zeta - \zeta_0\right)\right)}, \tag{8}$$

and f_{max} is its maximum value (in order to rescale the maximum of b to 1).

In equation (8), ζ_0 depends on the optimal elevation, namely, the elevation at which the vegetation is the most productive ($b(\zeta_0) = 1$ if $\lambda_1 = \lambda_2$), and λ_1 and λ_2 are parameters controlling the rate at which the biomass B tends to zero away from its maximum and can be chosen to be equal or different in order to depict a symmetric or asymmetric function, respectively.

In an attempt to investigate emergent geomorphic patterns in marshes characterized by different ecology across the world, we include two vegetation scenarios following *D'Alpaos et al.* [2007]. The first scenario (hereinafter referred to as vegetation type 1 scenario) portrays marshes colonized by pioneer species such as *Spartina Alterniflora*, characterizing the marshes located in the northeastern American coast, which typically appear as monospecific contexts. The second scenario (vegetation type 2 scenario) portrays marshes colonized by multiple species and characterizes the plant ecology of the majority of marshes worldwide.

Based on the findings of *Morris et al.* [2002], in the vegetation type 1 scenario (monospecific), the maximum biomass productivity is found close to the mean sea level; vegetation quickly dies back for lower marsh elevation due to increasing hypoxic conditions, while plant biomass progressively diminishes for higher elevation due to the reduction in the hydroperiod and frequency of flooding leading to accumulations of high concentrations of salt in pore waters. We therefore transcribe this relationship in the discontinuous formulation as follows:

$$b(\zeta) = \begin{cases} 0 & \text{if} \quad \zeta < \zeta_{min} \\ \frac{\zeta_{max} - \zeta}{\zeta_{max} - \zeta_{min}} & \text{if} \quad \zeta_{min} \le \zeta \le \zeta_{max} \\ 0 & \text{if} \quad \zeta > \zeta_{max} \end{cases} \tag{9}$$

where ζ_{min} is the minimum elevation at which *Spartina Alterniflora* starts colonizing the marsh platform and ζ_{max} is the maximum elevation that it can tolerate. In accordance with field observations [e.g., *Frey and Basan*, 1978], we set ζ_{min} = MSL (mean sea level) and ζ_{max} = HT (high tide).

On the contrary, field and remote sensing analyses of marshes covered by a variety of halophytic species provide evidence for the increase in species richness, hence vegetation biomass, with soil elevation [*Silvestri et al.*, 2005]. In this respect, in the case of vegetation type 2 scenario (multiple species), a different equation can be used:

$$b(\zeta) = \begin{cases} 0 & \text{if} \quad \zeta < \zeta_{min} \\ \frac{\zeta - \zeta_{min}}{\zeta_{max} - \zeta_{min}} & \text{if} \quad \zeta_{min} \le \zeta \le \zeta_{max} \\ 1 & \text{if} \quad \zeta > \zeta_{max} \end{cases} \tag{10}$$

where we set ζ_{min} = MSL and ζ_{max} = HT [*D'Alpaos et al.*, 2007].

To allow fair comparisons with the continuous formulation of equation (8), we set ζ_0 according to an optimal elevation equal to MSL and HT for the vegetation type 1 and type 2 scenarios, respectively. Figure 1 graphically represents the biomass density as a function of marsh elevation according to the two ecological scenarios (type 1 and type 2) and evaluated mathematically by means of the two considered formulations (continuous and discontinuous).

Other vegetation characteristics such as stem density n_s, stem diameter d_s, stem averaged height h_s, and projected plant area per unit volume a_s, come into play in some of the ecogeomorphic processes and need to be specified. On the basis of the long-term data set of *Spartina Alterniflora* productivity at. North Inlet estuary, USA [*Morris and Haskin*, 1990], *Mudd et al.* [2004, 2010] found that these plant morphometrics follow power law distributions as a function of vegetation biomass B, namely,

$$\begin{aligned} n_s &= \alpha_n B^{\beta_n}, \qquad h_s = \alpha_h B^{\beta_h}, \\ d_s &= \alpha_d B^{\beta_d}, \qquad a_s = \alpha_a B^{\beta_a}, \end{aligned} \tag{11}$$

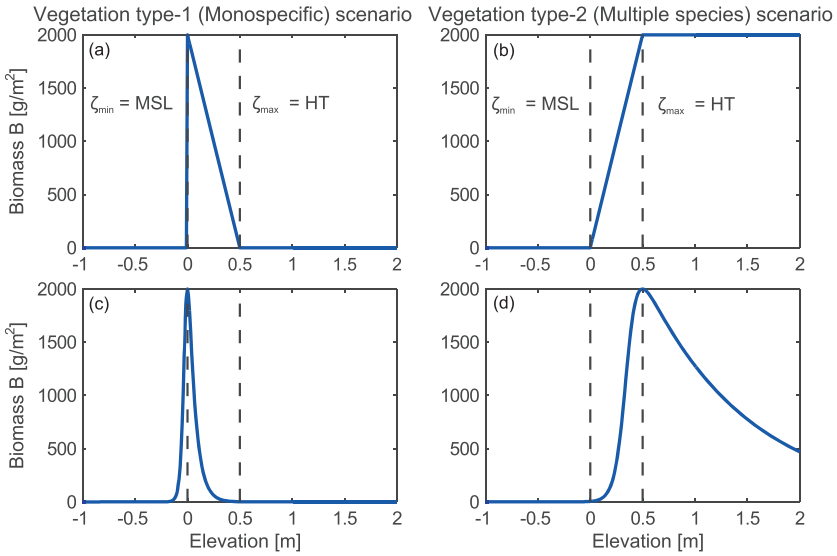

Figure 1. Vegetation biomass for the two ecological scenarios: (a and c) type 1, monospecific, and (b and d) type 2, multiple species, evaluated using the discontinuous formulation [*D'Alpaos et al.*, 2007] (Figures 1a and 1b) and the continuous function, modified after *Marani et al.* [2013] (Figures 1c and 1d).

where α_n, β_n, α_h, β_h, α_d, β_d, α_a, and β_a are empirical coefficients. Following *D'Alpaos et al.* [2007], we assume that similar relationships hold for the case of the marshes colonized by multiple species to allow a fair comparison between the two ecological scenarios.

Once the vegetation morphometrics have been evaluated, some of the ecogeomorphic processes, notably the ecosedimentary processes induced by the presence of the halophytic vegetation, can be formulated. Based on the approach of *Palmer et al.* [2004], the particle capture process Q_{dt} reads

$$Q_{dt} = CU\epsilon d_s n_s \min\left(h_s; Y\right),$$

with

$$\epsilon = \alpha_\epsilon \left(\frac{Ud_s}{\nu}\right)^{\beta_\epsilon} \left(\frac{d_{50}}{d_s}\right)^{\gamma_\epsilon}, \tag{12}$$

where $U = |\mathbf{U}|$ is the magnitude of the velocity, ϵ is a capture efficiency, describing the rate at which a particle in suspension is being trapped by plant stems, d_{50} is the mean particle size, ν is the water kinematic viscosity, and α_ϵ, β_ϵ, and γ_ϵ are empirical coefficients.

The second ecosedimentary process considered in equation (5) concerns the production of organic sediments, which can be related to the annually averaged aboveground plant dry biomass following the work of *Randerson* [1979]. Thereby, similar with *D'Alpaos et al.* [2007], we follow the formulation for the rate of organic sediment production Q_{db} proposed by *Mudd et al.* [2004], which yields

$$Q_{db} = Q_{db,0} b, \tag{13}$$

where $Q_{db,0}$ is a typical deposition rate derived empirically.

The third and last parameterized ecosedimentary process regards the enhanced settling of inorganic sediments. Indeed, in addition to the process of particle capture by plant stems, the concomitant influence of plants on velocity and turbulence during tidal flooding also participates in the settling of inorganic sediments, Q_{ds}. A number of researchers have found that these two hydrodynamic quantities tend to reduce with increasing stem density [*Leonard and Luther*, 1995; *Leonard and Croft*, 2006]. As customary in numerical models dealing with physical-biological interactions, we parameterize the flow resistance due to the presence of vegetation by means of the bed roughness to implicitly account for the effect of plant/flow interactions on

deposition. Therefore, in our model, the bottom shear stress is evaluated using the Gauckler-Strickler friction coefficient which, considering a total friction K_s, yields

$$K_s^{-2} = K_{s,g}^{-2} + K_{s,r}^{-2} + \phi K_{s,v}^{-2}, \tag{14}$$

where $K_{s,g}$ is the grain (or skin) roughness, $K_{s,r}$ is the roughness accounting for any irregular topography or macroroughness triggering local hydrodynamic dissipation, and $K_{s,v}$ accounts for the drag exerted by the vegetation, weighted by the parameter ϕ. Equation (14) directly follows from the assumption of an additive effect of these three components on the total shear stress τ that effectively acts in the hydrodynamic module (namely, $\tau = \tau_g + \tau_r + \phi\tau_v$, where the subscripts are consistent with the subdivision of K_s). When vegetation starts colonizing the marsh platform, ϕ increases leading to an increase in the last right-hand side term of equation (14) and so to a decrease in the effective total roughness K_s consequently. The decrease in K_s determines a decrease in the discharge per unit width $\mathbf{q}$, and as a consequence a reduced value of the bottom shear stress, eventually favoring the settling of inorganic sediments Q_{ds} included in equation (6). Since $K_{s,v}$ is mediated by the presence of biomass B, as a first approximation we assume that the weight factor linearly corresponds to the dimensionless biomass density, i.e., $\phi = b$.

Therefore, vegetation primarily contributes to surface sedimentation in the model by means of these ecosedimentary processes, whose rates highly depend on vegetation characteristics and notably on elevation-dependent vegetation productivity (i.e., biomass distribution in the tidal frame). However, other ecogeomorphic processes remain still poorly understood. For instance, most of the mathematical models simulating marsh platform evolution assume that the erosion flux Q_e vanishes over vegetated marsh platforms due to the impeded flow through the vegetation canopy, the resulting flow being too weak to produce excess shear stress and therefore net erosion. Although such an assumption stems from field observations [e.g., *Christiansen et al.*, 2000], it also poses the question of the dependence of the erosion rate on the spatial distribution and the density of the already established vegetation. Indeed, the conceptual model of *Yapp et al.* [1917] and the more recent contribution of *Temmerman et al.* [2007] indicate that vegetation distributed sparsely over the marsh platform in the form of hummocks promotes channel erosion, depicting a negative feedback between vegetation productivity and marsh elevation. Furthermore, *Bouma et al.* [2009] demonstrated in a laboratory experiment that the prevalence of one of the feedbacks over the other is a function of vegetation density. In view of these considerations, we assume that as a first approximation, the erosion decreases linearly as plant biomass increases, namely,

$$Q_e = Q_{e_0}\,(1 - b)\,, \tag{15}$$

This formulation, although simplified, retains the overall dynamics of this ecogeomorphic process.

2.3. Model Setup

The sets of numerical experiments were performed on a computational domain of dimensions 600 m × 400 m. The domain, although conceptual, seeks to be representative, by dimension, configuration, and bathymetry, of a typical shallow mudflat.

The initial bathymetry consists of an intertidal mudflat deprived of existing tidal networks and characterized by random (normally distributed) elevation perturbations ε. Different amplitudes and degrees of smoothness of these perturbations are tested (see Figure 2), but the mean bottom elevation on the mudflat is kept at a value $\zeta = -0.10$ m above MSL. The initial conditions are set for the free surface elevation ($\eta = 0$, corresponding to MSL), the velocity (still water), and for the suspended sediment concentration (SSC) ($C = 0$). We note that the effect of these initial conditions rapidly vanishes given the short length of the domain.

Three boundaries of the rectangular domain are closed, with no-flux conditions applied, whereas the seaward channel bordering the lower edge of the domain constitutes the open boundary where a semidiurnal sinusoidal tide with a reference amplitude a of 0.5 m (tidal range $R = 1$ m) is prescribed. This boundary condition is typical of tidal environments in microtidal regime (e.g., marshes in the Venice Lagoon), for which the underlying morphodynamic modeling framework was designed. Along the open boundary condition, a uniform and stationary SSC C_0 is also applied, mimicking the supply of sediments to the tidal basin, which enables us to consider different scenarios of concentration values.

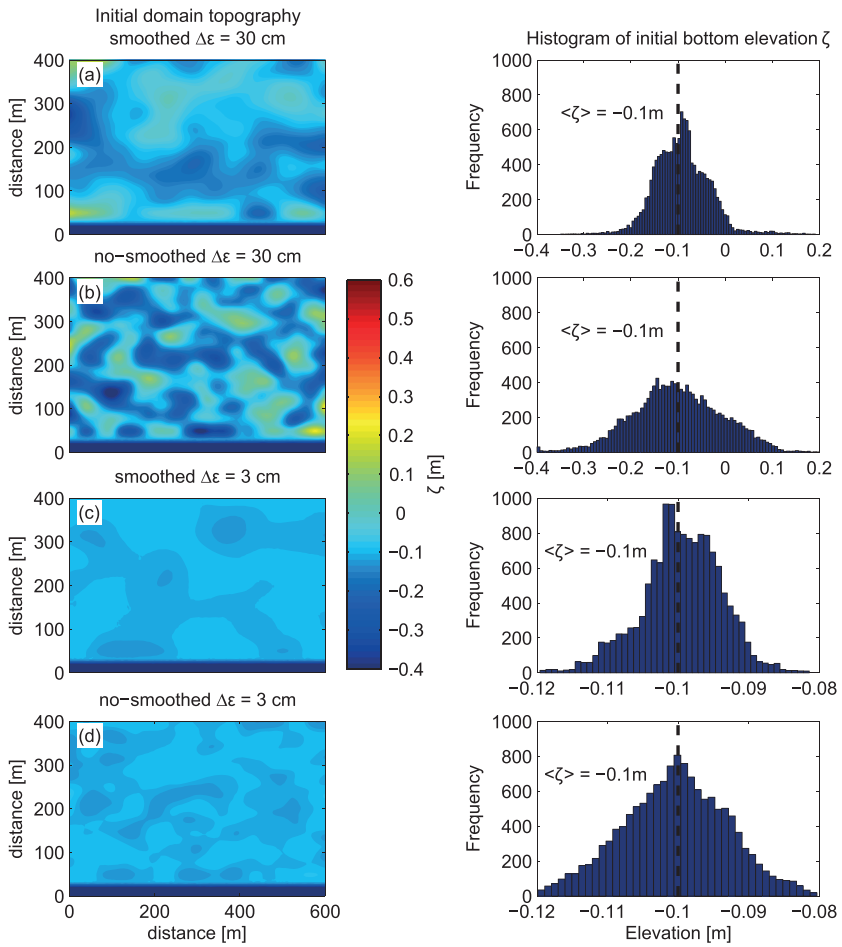

Figure 2. Four scenarios for the initial topographic configurations (left column) with their corresponding histograms of initial elevations ζ (right column), differing for the type of perturbations ε: (a) high and smoothed, (b) high and no-smoothed, (c) low and smoothed, and (d) low and no-smoothed.

The computational domain is discretized for the numerical solution using an unstructured triangular mesh with a mean element size of 5 m. The computational sequence at each time step proceeds as follows: (i) initial conditions provide information on the presence or absence of biomass and its related drag computed as in equation (14); (ii) the hydrodynamic equations are solved by means of a semi-implicit staggered finite element numerical scheme, which is based on the classical Galerkin variational method; (iii) the computed hydrodynamic field is fed into the sediment transport module in order to solve the advection-dispersion equation (1) and evaluate the different ecogeomorphic processes such as the ecosedimentary contributions in equations (12) and (13), eventually summed up to compute the global deposition flux in equation (5), while vegetation mediation on the erosion flux is determined based on equations (3) and (15).

The bottom topography usually evolves over a longer time than the hydrodynamics. This introduces the possibility to decouple the solution of the hydrodynamic field from the morphological evolution, an approach already implemented in several numerical modeling studies [e.g., *Marciano et al.*, 2005; *D'Alpaos et al.*, 2007; *Kirwan and Murray*, 2007; *Van Maanen et al.*, 2013a; *Schwarz et al.*, 2014]. Additionally, the computational effort required by the detailed hydrodynamic and sediment transport solvers makes impractical any long-term modeling application, unless the morphological changes, decoupled from the hydrodynamics, are artificially enhanced by using a "morphological factor." In the present modeling framework, the increase in the rate of the morphological change is determined through a so-called "offline" method, as opposed to the "online" method [*Roelvink*, 2006]. This method consists of multiplying the bed level changes integrated over a tidal cycle by a morphological factor M. This choice corresponds to adopt a morphodynamic time step for the evolution of bottom elevations given by M times the tidal period. Bottom elevations are therefore updated, resulting in a new topographic configuration and consequently a new spatial biomass distribution. Then, a

Table 1. Values of Parameters Used in the Simulations

Parameter	Value	Reference	Parameter	Value	Reference
$\tau_{cr,e}$	0.4 Pa	*D'Alpaos et al.* [2006]	γ_ϵ	2.08	*Palmer et al.* [2004]
$\tau_{cr,d}$	0.1 Pa	*Amos et al.* [2004]	α_a	0.25 m g^{-1}	*Mudd et al.* [2004]
d_{50}	20 μm	*Amos et al.* [2004]	β_a	0.5	*Mudd et al.* [2004]
p	0.4	*D'Alpaos et al.* [2007]	α_d	0.0006 m^3 g^{-1}	*Gibbs* [1985]
$K_{s,v}$	15 $m^{1/3}$ s^{-1}	*Chow* [1959]	β_d	0.3	*Fagherazzi and Furbish* [2001]
$Q_{db,0}$	0.002 m yr^{-1}	*D'Alpaos et al.* [2006]	α_n	250 g^{-1}	*Mudd et al.* [2004]
B_{max}	2000 g m^{-2}	*D'Alpaos et al.* [2007]	β_n	0.3032	*Mudd et al.* [2004]
α_ϵ	0.224	*Palmer et al.* [2004]	α_h	0.0609 m^3 g^{-1}	*Gibbs* [1985]
β_ϵ	0.718	*Palmer et al.* [2004]	β_h	0.1876	*Fagherazzi and Furbish* [2001]
$\Delta\zeta_{ref}$	0.005 m		w_s	0.00034 m s^{-1}	
ζ_0 (vegetation type 1)	−0.0183		ζ_0 (vegetation type 2)	0.34785	
λ_1 (vegetation type 1)	15		λ_1 (vegetation type 2)	1	
λ_2 (vegetation type 1)	45		λ_2 (vegetation type 2)	18	

new morphodynamic iteration can be carried out. This computational sequence is summarized in Figure S1 in the supporting information.

The morphological factor M is adjusted at every morphodynamic time step considering the actual bed change in relation to a reference value estimated as acceptable. Hence,

$$M = \frac{\Delta\zeta_{ref}}{\Delta\zeta_{max}}, \tag{16}$$

where $\Delta\zeta_{max}$ is the maximum integrated bed level change over a tidal cycle found within the domain and $\Delta\zeta_{ref}$ is the maximum accepted change. Indeed, we assume that any morphological change lower than $\Delta\zeta_{ref}$ does not significantly affect the hydrodynamic computation during a tidal cycle, thus allowing for the theoretical repetition of the same hydrodynamic forcing determining the fluxes of sediments from and to the bottom (i.e., Q_e and Q_d).

The determination of $\Delta\zeta_{ref}$ was based on a sensitivity analysis of the numerical results. We applied different values of M to update the bed topography after a computed tidal cycle. Then, we compared several statistics (e.g., absolute and relative errors) of the main hydrodynamic variables (bed shear stress and the magnitude of the velocity) calculated during a new tidal cycle in two cases: with $M = 1$ and with an arbitrary value of M. Such an investigation was performed using different underlying topographic configurations in order to assess the possible dependence of $\Delta\zeta_{ref}$ over different morphodynamic regimes. This method allows one to adapt M to different morphodynamic rates of change in the various marsh evolutionary stages (we found a maximum value of $M \simeq 5$, 10, and 90 for topographic configurations with semideveloped, with highly developed, and without tidal networks, respectively) so that the morphodynamic time step varies throughout the simulation period. Typically, M is small during the first model iterations but rapidly increases until it reaches a stable value (see Figure S2).

Every simulation is run for a period of 30 years to obtain information on both channel initiation and further stages of elaboration. When relevant, results are also presented for 100 year computations to give perspective over the long term. The values of the physical and empirical parameters adopted throughout the different simulation sets are listed in Table 1.

3. Results

In the following we illustrate the results of a series of simulations exploring first the role of sediment supply and the effect of vegetation type on tidal network formation and further elaboration. In a second stage, the investigation is devoted to the role of the initial topography on tidal network development. This choice of forcing factors is meant to highlight the influence of specific boundary and initial conditions, which are thought to control tidal channel morphodynamics.

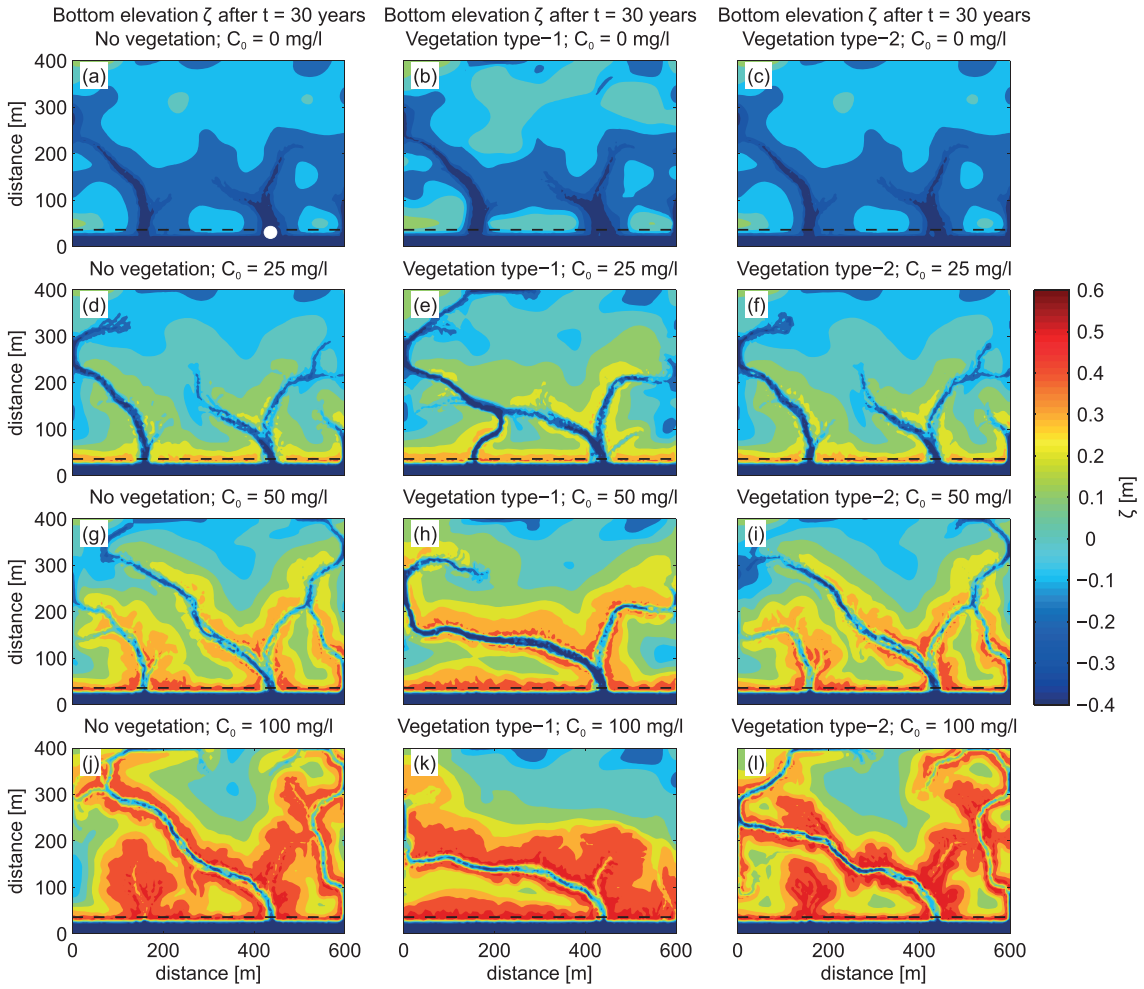

Figure 3. Simulated marsh morphologies after 30 years according to different sediment supply and marsh ecology, computed with the continuous formulation (see equation (8)). Columns: with different ecological scenarios; rows: with increasing sediment supply. Marsh morphologies developed from a tidal flat characterized by high and smoothed topographic perturbations (i.e., Figure 2a). The white dot displayed in Figure 3a refers to locations at which the channel cross-sectional area and the tidal prism are computed and their values presented in subsequent figures.

3.1. Role of Sediment Supply

The main set of simulations was devoted to analyze the effect of the sediment supply. An overview of the results is provided in Figure 3, which displays final plan view morphologies starting from an initial mudflat characterized by high and smoothed perturbations ε (i.e., Figure 2a) and forced under different scenarios of sediment supply (rows are distinguished by the different values of the input SSC C_0, ranging from 0 to 100 mg/L) and marsh ecology (the different columns refer to the case without vegetation, with vegetation type 1 and type 2, respectively). In this set of simulations, biomass distribution is estimated by means of the continuous formulation (see Figures 1c and 1d).

A variety of erosional and depositional mechanisms emerges from Figure 3, which highlights how the properties of the resulting tidal networks change depending on sediment supply and vegetation type. Looking at the overall planforms, the sedimentation patterns, which increase with the sediment supply, are largely influenced by the course of the forming tidal channels and progressively decrease away from them (e.g., Figure 3l). Such a spatial distribution suggests that tidal waters and incoming suspended sediments are chiefly transported through the forming tidal channels rather than as sheet flow [*Temmerman et al.*, 2005]. This hydrodynamics is consistent with flow regimes typically occurring in shallow basins under microtidal conditions.

The resulting marsh morphologies characterized by concave-up marsh platforms dissected by channels with high elevated levees are conformed with field observations of microtidal marshes either grown by single-plant

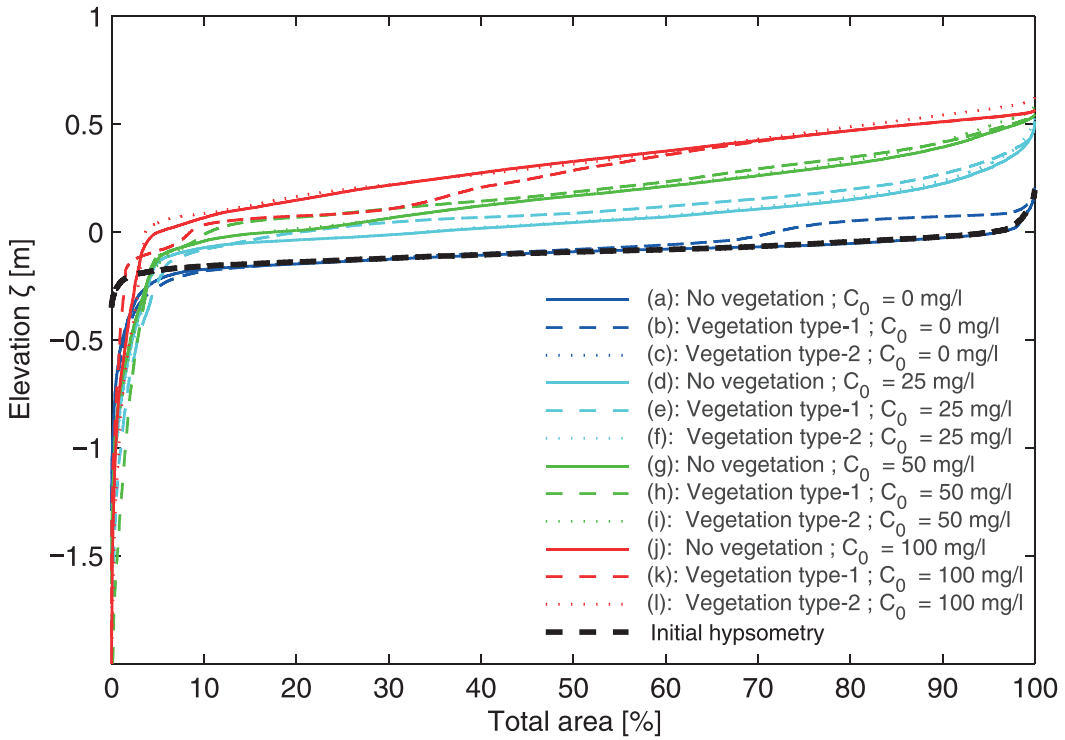

Figure 4. Hypsometric curves of the whole tidal basin for the simulated marsh morphologies after 30 years.

communities such as in North Inlet, USA [e.g., *Morris et al.*, 2005; *Torres and Styles*, 2007], or by multiple species such as in the Venice Lagoon, Italy [e.g., *Marani et al.*, 2004; *Silvestri et al.*, 2005; *Wang et al.*, 2009].

We also note the formation of tidal channels in all of the considered scenarios, although with different planimetric and bathymetric characteristics. The channel plan view morphologies evoke an increase in channel maturity with increasing sediment supply. As a matter of fact, while hydraulic path geometry in Figures 3a–3c materializes the presence of ill-defined tidal channels characterized by shelving banks, more clearly defined course features with marked banks describe, on the contrary, tidal channels developing under scenarios characterized by increasing sediment supply. The corresponding tidal networks also portray a higher degree of channel lengthening and sinuosity suggesting an increase in channel complexity with sediment supply. Signs of channel senescence depict tidal networks developed under high incoming SSC such as channel narrowing and even low-order creek closure by sediment infilling (e.g., Figures 3j–3l). These observations suggest that the simulated tidal networks, although developing in every simulation run, may be considered in different evolutionary stages. With longer marsh development (see Figure S3), these dynamics are further pronounced. Marshes under high sediment supply continue to accrete vertically and prograde horizontally, which further contract the embedded tidal networks. The tidal prism conveyed via the channels is progressively reduced, channel persistence does no longer prevail, and channels become infilled ultimately. Conversely, despite the absence of sediment supply, marsh morphologies characterized by $C_0 = 0$ mg/L portray small morphological changes over the longer term, notably materialized by the low headward expansion of the tidal networks, which can be inferred to the rather low tidal hydrodynamics at work.

Figure 4 displays the integrated hypsometries of the final morphologies and suggests that different platform and channel morphological characteristics occur. The growing upward shift of the hypsometric curves with increasing sediment supply alludes to the progressive aggradation of the marsh platform. The curves also tend to progressively loose the typical sigmoid shape toward the development of a linear profile followed by a sharp discontinuity. This is due to the transition from an initially perturbed topography characterized by depressions and rising ground features to a relatively flat topography being undercut by marked discontinuities represented by the presence of mature channels with distinct natural levees and therefore corroborating with the observations from Figure 3.

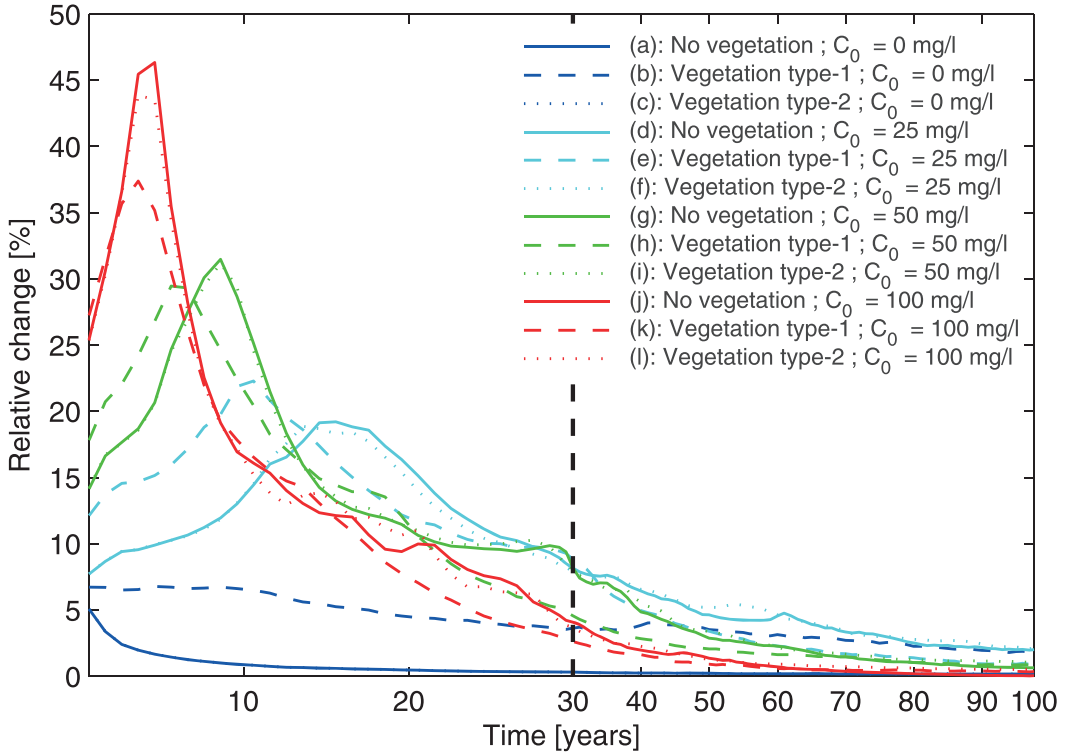

Figure 5. Relative change of averaged bottom elevation between consecutive years expressed in percentage for the simulated morphologies. The time scale is compressed after the 30 year basic simulation period highlighted by the dashed line.

Figure 5 shows the temporal evolution of the relative change of averaged bottom elevations, namely, the absolute difference between two consecutive years scaled by the starting year, expressed in percentage. A focus is made over the basic simulation period (i.e., 30 years), along with insights into the longer term (using a different time scale in the plot). Indeed, during the first decades, morphological changes within the tidal basin are significant and appear to occur not only earlier but also higher in magnitude with increasing sediment supply regardless of the ecological scenarios. These changes progressively slow down in time until they become negligible after 100 years for nearly all scenarios. Figure 5 thus supports the assumption that a 30 year period is sufficient to study the formation and early development of tidal networks because most of the morphodynamic activity arises in the first 20 years, when the geomorphic properties are already well defined. Over the longer term (100 years), all the different trends depicted in Figure 5 allude to the convergence toward a state with relatively low elevation changes. Yet the design and setup of our model that involves ecogeomorphic processes (with both inorganic and organic deposition), as well as continuously incoming sediment fluxes, prevent morphodynamic equilibrium to occur in the form that can be observed in nature. Alternately, the equilibrium observed here corresponds to a completely infilled basin in a way that the morphological stable configuration experienced by the different simulations is associated with marshes characterized by elevations that everywhere asymptotically tend to the elevation of the highest tidal level, rather than a dynamic equilibrium with local hydrodynamics corresponding to marsh surfaces at a given elevation within the tidal frame (e.g., between MSL and HT), as observed in nature. In addition, the production of organic sediments allows the marsh platform to accrete even above the level of HT, thus out of the intertidal zone, forcing the marsh to become low supratidal. This comparison further supports the observation that the synthetic tidal networks across the different simulation cases are in different evolutionary stages.

3.2. Effect of Vegetation Type

The comparison between scenarios characterized by different ecological features in Figure 3 points out the importance of vegetation type in driving the overall morphodynamic evolution of the intertidal platform together with its biogeomorphic features. Notable differences in marsh and channel plan view morphologies arise when comparing simulations without vegetation (i.e., Figures 3d, 3g, and 3j) and those characteristic

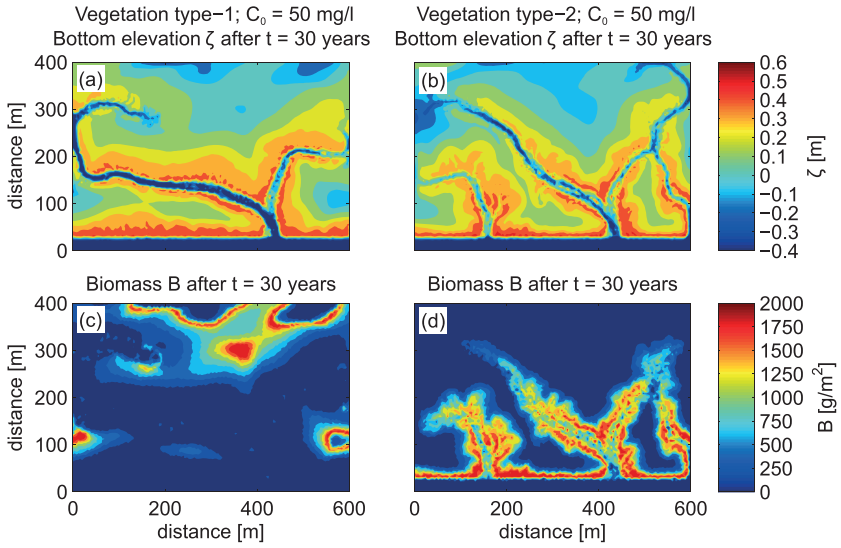

Figure 6. Spatial biomass distribution for the simulated marsh morphologies in Figures 3h and 3i after 30 years.

with the type 1 (monospecific) vegetation scenario (i.e., Figures 3e, 3h, and 3k). These distinctions mainly depend on the strong influence of this type of vegetation, which is denser at a lower bed elevation, in the initial process of channel formation. On the other hand, although local differences take place, the overall channel morphology remains fairly similar between simulations without vegetation and those characterized by the type 2 (multiple species) vegetation scenario (i.e., Figures 3f, 3i, and 3l), changes mainly regarding the presence of lateral shifts in channel location and elongation.

Figure 6 compares the spatial distribution of bottom elevation and biomass for the cases in Figures 3h and 3i ($C_0 = 50$ mg/L). The different ecological scenarios induce, in particular, distinct patterns of spatial biomass distribution. In marshes colonized by monospecific vegetation species such as *Spartina Alterniflora*, vegetated areas are pushed back to the landward side of the tidal basin (Figure 6c). This landward migration is explained by the negative relationship between plant productivity and marsh elevation that applies above MSL in the vegetation type 1 scenario, as graphically illustrated in Figure 1c. Indeed, sedimentation decreases with distance from the seaward channel and from the forming tidal channels as a result of the decrease in sediment deposition due to the reduction of the advective transport and hydroperiod. As a consequence, regions near the seaward channel, where the incoming flux of sediments originates, experience the highest sedimentation rates during the first simulation years, thus showing a strong feedback between morphological changes and vegetation growth. The following elevation gain leads to the progressive disappearance of the already established pioneer species. Moreover, the forming channels promote the transport and subsequent deposition of suspended sediments further landward, eventually constraining vegetation to regions not yet dissected by tidal channels, as it emerges from Figure 6a.

Conversely, due to the positive relationship linking biomass and marsh elevation that holds until HT in the type 2 (multiple species, Figure 1d) vegetation scenario, maximum biomass productivity is found in proximity of the tidal channels. As a matter of fact, once channels have developed, the enhanced deposition process becomes an inverse function of the hydraulic distance from them. Accordingly, it is maximal near the channels owing to the high magnitude of the advective fluxes and progressively decreases as moving away from the channel banks. The local accretion alongside the tidal channels produces favorable conditions for plant growth, which in turn enhances further sedimentation. Biomass patterns following the forming tidal courses (see Figure 6d) are a clear manifestation of these biophysical dynamics, in agreement with field observations. Thus, the model correctly reproduces the well-documented positive feedback mechanism between marsh elevation and plant productivity for marshes colonized by multiple species. These different vegetation spatial distributions induce distinctions in the flow and concentration fields as illustrated in Figure S4 which exhibits the spatial distributions of the magnitude of velocity and SSC at a particular instant during the flood phase. Considering vegetation type 2 scenario, vegetation biomass establishes seaward and alongside the main channels (Figure 6b) which constricts tidal flows in the channel due to the corresponding high elevated

channel levees, coupled with the enhanced flow resistance provided by the vegetation, as also suggested by *D'Alpaos et al.* [2006]. Therefore, tidal channels experience higher velocities all over their courses as compared with simulation cases in the absence of vegetation (see Figures S4a and S4c), and a sensibly higher landward transport of suspended sediments occurs consequently (see Figures S4d and S4f). The differences in marsh and channel morphologies characterizing vegetation type 1 simulations make difficult to draw comparisons with the other ecological scenarios.

One can clearly distinguish the marked effect of vegetation in enhancing sediment deposition also looking at the hypsometries of the simulated morphologies (see Figure 4). For instance, the sudden bump in curve (b) around MSL is clearly a manifestation of the production of organic sediments, which is the only depositional mechanism in this simulation due to the absence of inflowing SSC ($C_0 = 0$). Such ecosedimentary processes are highlighted by this step-like pattern in some of the hypsometric curves (e.g., curves (h) and (k)). For a same sediment supply scenario, the hypsometry featuring tidal basins grown by single species (vegetation type 1) depicts the highest elevation with increasing domain area except for tidal basins under high accretional activity (e.g., compare curve (k) with respect to curves (j) and (l)). This peculiarity can be illustrated looking at the corresponding plan view morphology of the specific case (k), (see Figure 3k), where the presence of a barrier-like depositional feature in the middle of the domain obstructs the headward extension of the tidal network further landward. This large low-lying marsh area is thus subject to little accretion over the simulation period, which explains why the integrated elevation for the same percentage area is lower for this scenario compared to the two other ecological scenarios.

3.3. Network Statistics

A further analysis was performed to assess whether the synthetic tidal networks meet observed network statistical metrics in order to quantitatively validate the modeling framework. Figure 7 reports on the mouth minimum cross-sectional area Ω, i.e., computed below MSL, of the tidal network common to all the simulated morphologies (see white dot in Figure 3a) against the tidal prism P flowing through the corresponding outlet and evaluated at $t = 30$ years. Data in Figure 7 are arranged in two clusters: a first cluster gathering the simulation cases with no external sediment supply and a second one comprising the remaining simulation cases. This clustering clearly results from the distinct character of the simulated morphologies in the absence of sediment supply which becomes reflected in the channel cross-sectional geometries. Indeed, as these morphologies are not supplied by external sediments, levees cannot form, which hinder channel growth. Alternately, poorly defined drainage courses with undefined channel banks develop after 30 years as noticed in Figures 3a–3c, thus explaining the significant differences in cross-sectional areas as compared with the other simulated morphologies.

A regression analysis between P and Ω performed on the second cluster shows that the data can be approximated by a power law regression model, in agreement with the well-established O'Brien-Jarrett-Marchi (O'BJM) law [e.g., *D'Alpaos et al.*, 2010; *Toffolon and Lanzoni*, 2010]:

$$\Omega = kP^{\alpha}, \tag{17}$$

where k and α are empirical coefficients. The value of the exponent α (see Figure 7) lies in the range 0.85–1.10 in accordance with the empirical law [*O'Brien*, 1969; *Jarrett*, 1976].

This scaling relationship provides a synthesis of the complex and site-specific feedbacks occurring between tidal channel geometry and tidal hydrodynamic regime. Particularly, equation (17) implies that channel cross-sections are in dynamic equilibrium with the local tidal prism [*D'Alpaos et al.*, 2010]. Accordingly, tidal networks developed under sediment-poor context (i.e., absence of sediment supply) have not achieved an equilibrium condition after 30 years. The temporal evolution of the geomorphic relationship between Ω and P over the basic simulation period (i.e., 30 years) is also examined in Figure 8. A clear distinction emerges again between the simulations under marsh retrogradation and those in marsh progradation contexts. Regardless of the ecological scenario, the channel cross-sectional area Ω for the three runs with no sediment supply (i.e., Figures 8a–8c) increases throughout the simulation period. On the contrary, a global decrease with time in Ω and P characterizes the simulation cases with high sediment supply.

An overall gradient from channel scouring toward progressive channel infilling is covered by the set of different simulations. These two contrasting processes acting on the morphological evolution of tidal channels imply that the synthetic tidal networks are in different morphological ages. More precisely, the time evolution of the relationship between Ω and P for simulations under high sediment supply exhibits an increase for

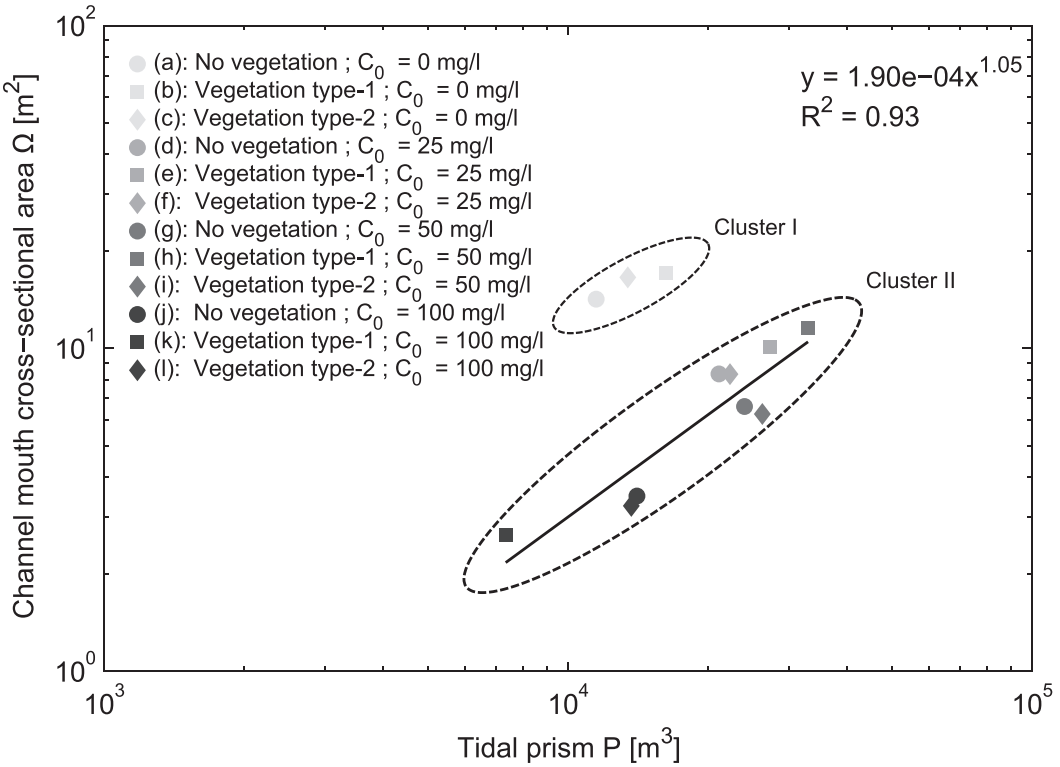

Figure 7. Log-log plot of the total cross-sectional area Ω versus tidal prism *P* at the mouth of the tidal network channels common to the simulated marsh morphologies (see Figure 3a) after 30 years.

the first years followed by a decrease until the end of the simulation period. In this latter period, the data may be approximated by a power law (e.g., Figures 8j–8l). Such a pattern is qualitatively consistent with a similar investigation reported in *D'Alpaos et al.* [2010]. Exploring the coevolution of Ω and *P* over 100 years, as displayed in Figure S5, further emphasizes the progressive infilling of the network mouth for the simulation cases with sediment supply, which leads to the invalidity of the O'BJM relation over the longer term. These results show that 30 years represent a relevant time scale to reach a well-defined channel imprinting in accretional contexts and to study their geomorphic properties.

Another geomorphic measure looks at the drainage density of the synthetic tidal networks. According to *Marani et al.* [2003], the conventional Hortonian metrics appear to be unable to distinguish peculiarities in tidal network structures. Instead, site-specific features and important differences in network morphologies may only be captured by evaluating the unchanneled flow lengths *l* within the domain, namely, the distance from any marsh point to the nearest channel. In tidal networks, determining such a measure requires the definition of flow directions on the basis of hydrodynamic rather than topographic gradients. In the present contribution, we use the method proposed by *Rinaldo et al.* [1999], which consists of suitably simplifying the classical shallow water equations to a Poisson boundary value problem to solve the free surface elevations and thereby deduce drainage directions through the associated gradients.

Figure 9 displays the semilog plot of the exceedance probability of the unchanneled flow lengths ($P \geq l$) for the various simulated marsh morphologies. The statistical properties allow to perceive the tidal network capability to drain its basin and therefore provide an appropriate definition of drainage density. The approximate linear trend of the curves alludes to exponential probability distributions and therefore a pointed absence of scale-free properties in network structures. Such a property implies that the synthetic tidal networks lack scale invariance features, a characteristic of fractals yet common to their fluvial counterpart, in agreement with previous studies [*Marani et al.*, 2003; *Feola et al.*, 2005].

Furthermore, apart from the simulation case characterized by $C = 100$ mg/L with vegetation type 1 scenario (i.e., distribution (k)), the overall results point out to a decrease in the mean unchanneled flow length *l*, hence an increase in the drainage density, as the sediment supply increases. Such an observation reflects that the

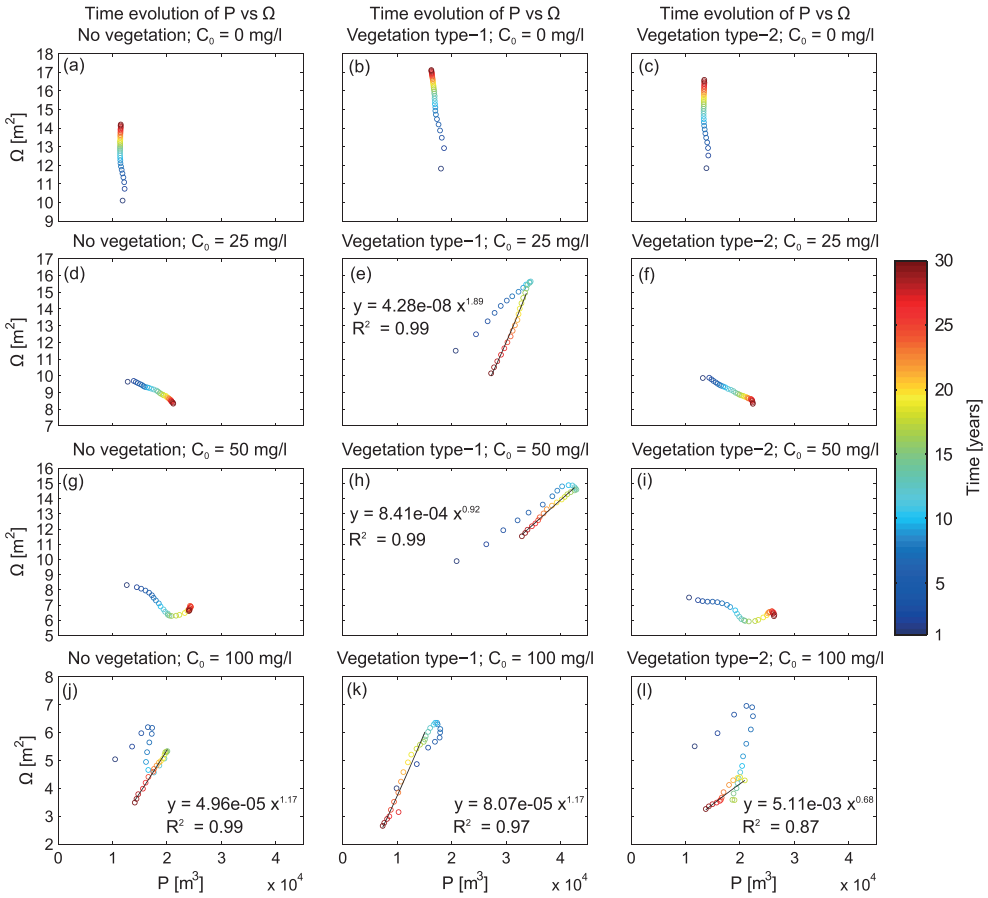

Figure 8. Time evolution of the total cross-sectional area Ω versus tidal prism *P* at the mouth of the tidal network channels common to the simulated marsh morphologies (see Figure 3a).

various synthetic tidal networks present different degrees of elaboration/complexity, and so different evolutionary stages, corroborating the previous results. The departure of the distribution (k) from this general relationship may be explained by the fact that the respective tidal network presents a course location that is restricted to the lower left region of the domain (see Figure 3k) because of the barrier-like structure produced by the intense deposition interacting with vegetation. Such a structure leaves a large portion of the tidal basin unchanneled and consequently high unchanneled flow lengths.

The procedure employed to assess this metric should be yet taken with precaution. Indeed, the Poisson boundary value problem used to solve the flow patterns is in theory limited to cases where the fluctuations of unchanneled area bottom elevation around its mean are significantly smaller than the instantaneous average water depth [*D'Alpaos et al.*, 2005]. Consequently, this Poisson problem would predict that water would tend to flow toward the nearest tidal channels. However, the present morphologies portray variations in bottom elevations that are comparable or even larger than the water depth across the unchanneled area. Such variations are present because the simulated morphologies are building up in the tidal frame. That being said, the results obtained through the Poisson model still agree with the network characteristics observed in Figure 3; i.e., the longest tidal networks correspond to the highest drainage density.

3.4. Role of Initial Bathymetry

A further step of our analysis was devoted to investigating the influence of initial conditions on tidal network development. Figure 10 shows final (30 years) plan view morphologies obtained starting from the four initial topographic configurations displayed in Figure 2, keeping the three ecological scenarios but with a constant value of SSC $C_0 = 50$ mg/L.

The diversity in final morphologies is indicative of the crucial role of the initial topography in driving tidal channel morphodynamics. Indeed, network lengthening, sinuosity, and complexity highly differ within this

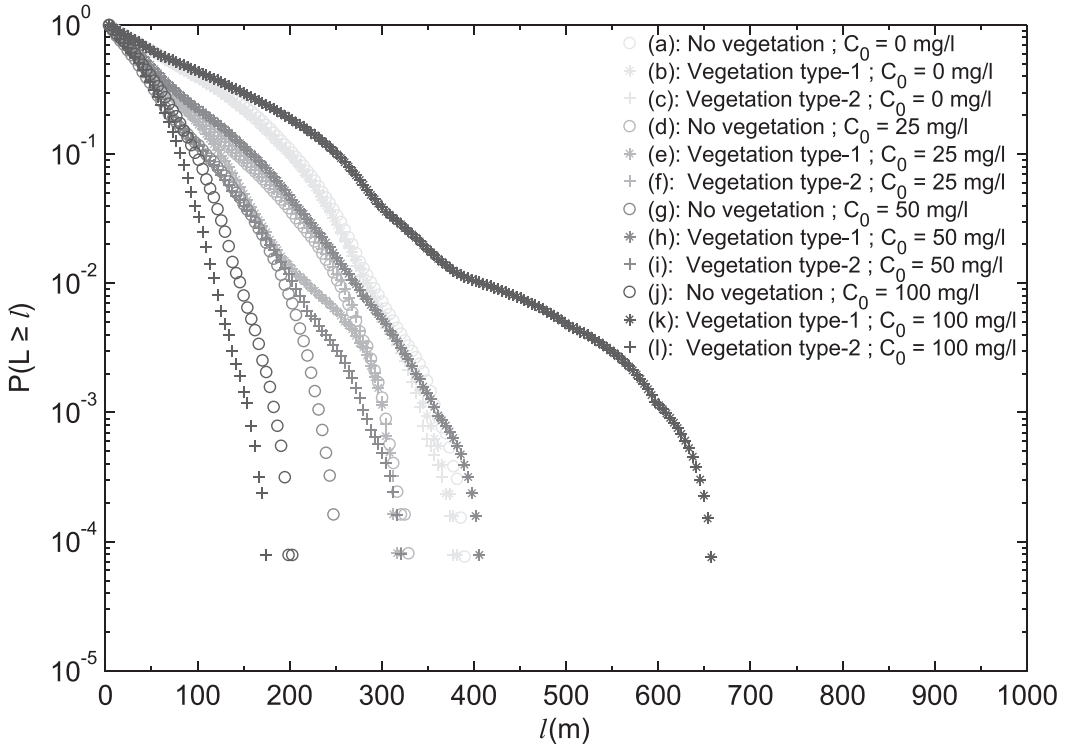

Figure 9. Semilog plot of the exceedance probability of unchanneled flow lengths ($P \geq l$) for the synthetic tidal networks of the simulated marsh morphologies after 30 years. The approximate linear trends suggest an exponential distribution whose slope represents the mean unchanneled flow length, while the drainage density is estimated by its inverse value.

simulation set. Precisely, the amplitude of the initial topographic perturbations ε seems to influence tidal network characteristics with a notable increase in channel density and complexity as the height of the topographic noises increases.

The degree of smoothness of these perturbations may affect the planform patterns with the presence of more sinuous tidal channels as the topography becomes rougher; see Figures 10d–10f compared to Figures 10a–10c, both series with $\Delta\varepsilon = 30$ cm. Yet this seems to be still a function of the size of the initial perturbations as the degree of smoothness no longer influences channel morphology when the perturbation amplitude is low (e.g., Figures 10g–10l with $\Delta\varepsilon = 3$ cm).

Overall, results emphasize that network morphological evolution and complexity occur more rapidly and in greater extent when tidal channels develop onto an initial highly perturbed bathymetry.

4. Discussion

The various numerical experiments bring interesting results that are worth to be further discussed. First, Figure 3 exhibits the formation and evolution of tidal networks throughout the range of sedimentary and ecological scenarios investigated, which yet result from different morphological processes. Figure 11 brings further insights into this concern. The different subplots display the time evolution of a cross-sectional profile for the simulated morphologies (the location is highlighted by the dashed line in Figure 3). Results point out that channel deepening results from the progressive bottom scouring for the simulations in the absence of sediment supply (Figures 11a–11c), whereas it chiefly results from the continuous aggradation and progradation of the flanking marsh platform for the simulations with high sediment supply (e.g., Figures 11j–11l).

Such observations constitute good testimonies of the occurrence of two channel-forming processes: differential erosional formation in marsh retrogradation context and differential depositional formation in marsh progradation context [*Stefanon et al.*, 2010, 2012]. Nevertheless, a detailed examination of Figure 11 evokes a

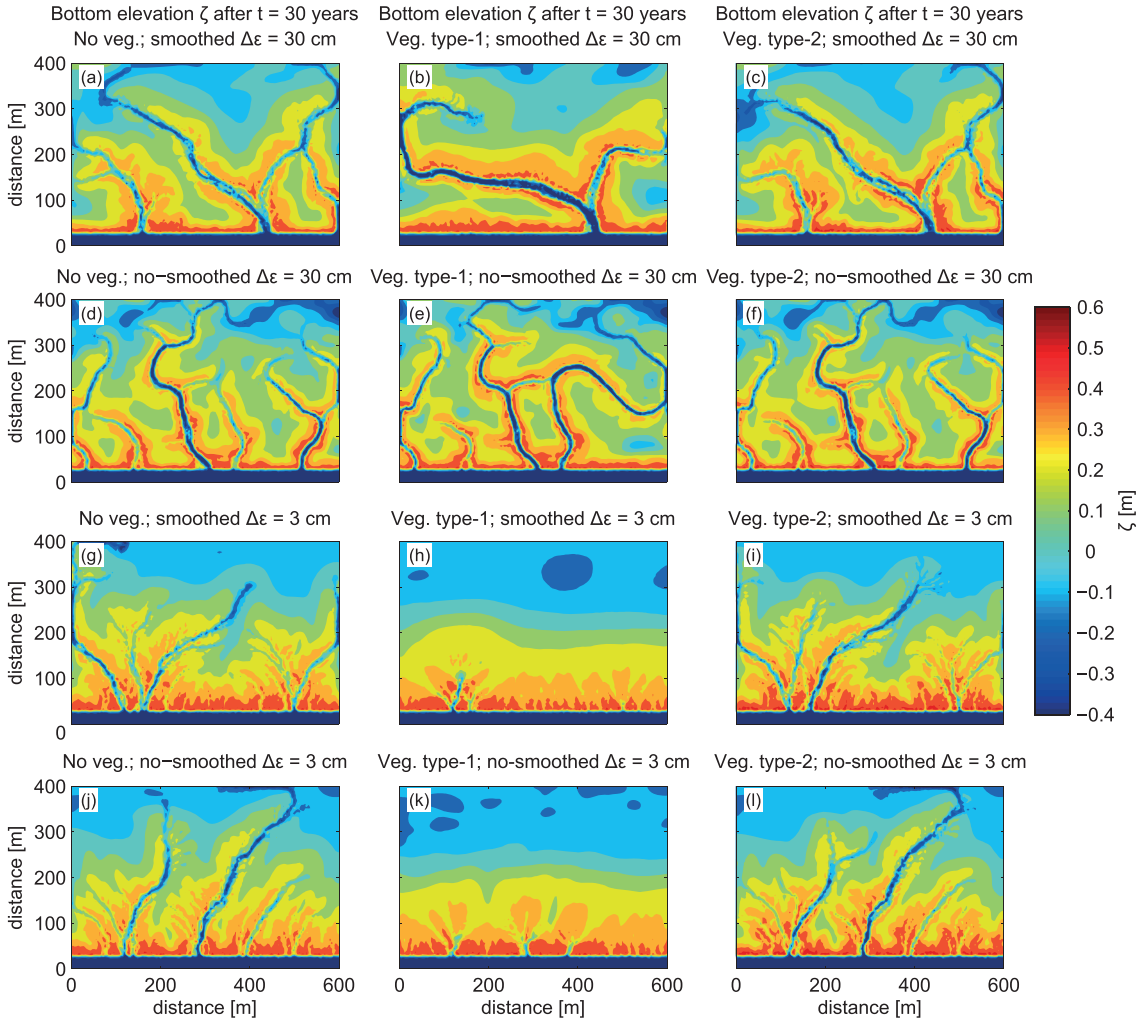

Figure 10. Simulated marsh morphologies after 30 years under a sediment supply $C_0 = 50$ mg/L for different initial topographic configurations and marsh ecological scenarios, computed with the continuous formulation (8). Columns: different ecological scenarios; rows: different amplitudes and degree of smoothness of initial perturbation reported in Figure 2.

more complex picture of the problem. As a matter of fact, throughout the different simulations, the mouth of the main tidal network, which represents the outlet of the common subbasin examined in previous figures, occurs at the same location where an initial topographic depression exists. This analogy suggests a similar underlying mechanism participating in channel initiation regardless of the sedimentary and ecological contexts. Indeed, here channel initiation is ascribed to the incision process as a result of flux concentration into the local initial depression producing excess bed shear stress.

Recalling the global picture of tidal network ontogeny, the different interpretations indicate that for tidal networks developing under high accretional activity, the two channel-forming processes in reality coexist but act at different time scales. Channel formation is attributed to the erosional process of channel incision that gives a basic imprinting to the network, in line with previous observations [e.g., *Beeftink*, 1966; *French and Stoddart*, 1992] and modeling studies [e.g., *Fagherazzi et al.*, 2004; *D'Alpaos et al.*, 2005]. Then, channel incision and headward erosion occur during channel elaboration together with the prevalent depositional process of differential deposition, contributing to channel deepening. Eventually, channel narrowing, segmentation, and even closure, due to the further aggradation and progradation of the marsh platform, represent other depositional processes acting over the longer time scales where depositional processes cancel out erosion.

Fundamentally, tidal creeks, channels and the encompassing networks, are believed to experience three main ontogenic (or evolutionary) stages, namely, initiation, elaboration, and integration (or reduction) [*Steel and Pye*, 1997; *Allen*, 2000]. Conventionally, while channel initiation and integration represent the

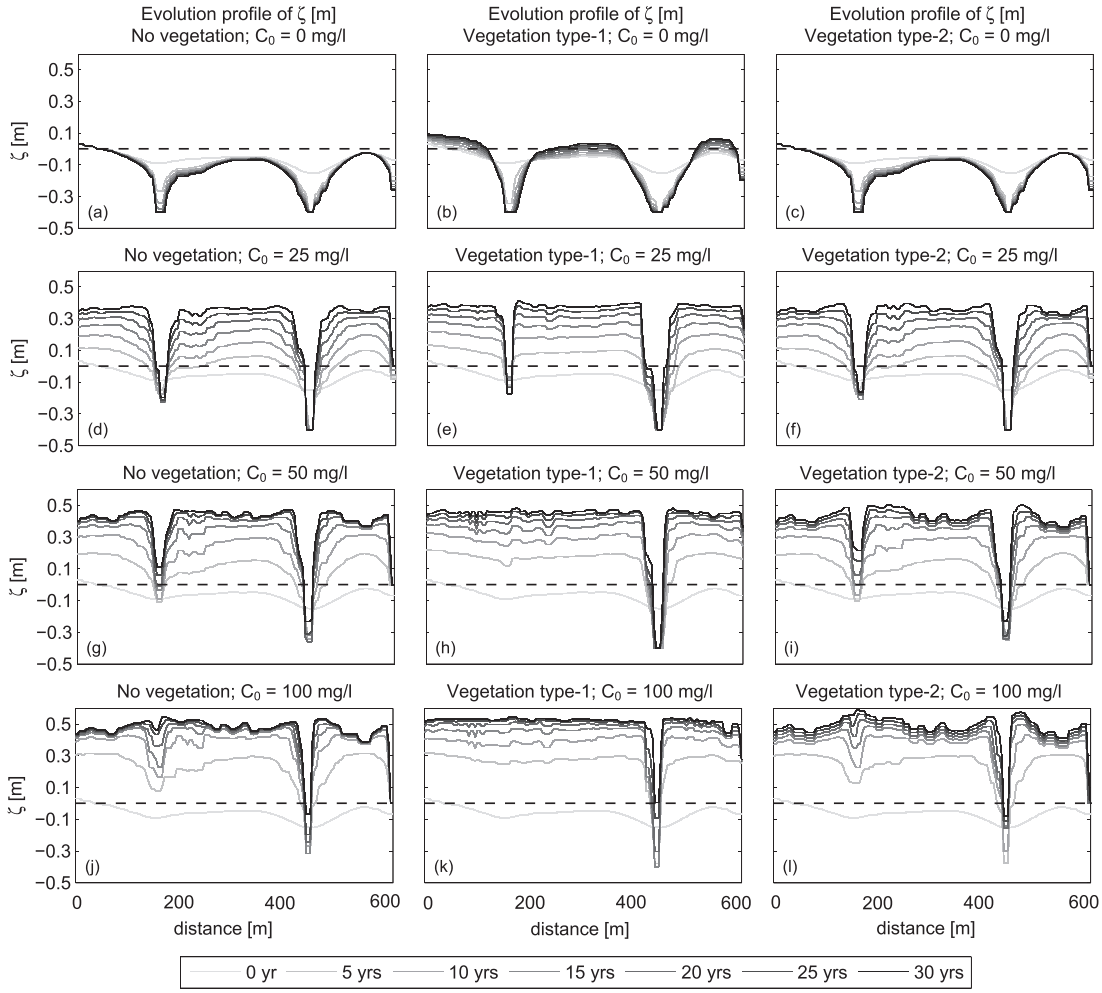

Figure 11. Time evolution of a cross-sectional profile (see dashed line in Figure 3) for the simulated morphologies.

respective initial and final channel ontogenic stages, sometimes the elaboration stage constitutes itself a phase or a manifestation of a more global intermediate stage including also the elongation and extension phases as in *Glock* [1931]. A direct example is provided in Figure 12, which depicts the temporal evolution, over a 100 year period, of the tidal basin, considering a SSC $C_0 = 100$ mg/L and vegetation type 2 scenario, and whose morphology after 30 years was displayed in Figure 3l. Tidal network initiation takes place within the first years when a few ill-defined drainage patterns appear (see Figure 12b). Network elaboration comes then into play through progressive channel landward extension and locally low-order tidal creek initiation until the networks reach their maximum extents after about 30 years (see Figure 12d). Henceforth, signs of channel senescence arise such as continuous narrowing of the main channels until their completed infilling after 100 years (see Figure 12k). These latter processes are indicative of network integration.

The present analyses suggest that tidal network ontogeny is accelerated in marsh accretional context. Various results justify this interpretation. For instance, the qualitative observations from Figure 3 depict higher degree of channel lengthening as the sediment supply increases, which alludes to more elaborated channels as opposed to the presence of young ill-defined channels when sediment supply is limited. Furthermore, the channel senescence features such as channel narrowing and low-order creek infilling portrayed in the highest accretional scenarios in Figure 3 denote that tidal networks have gone beyond maturity, and start experiencing a reduction (or integration) evolutionary stage, in agreement with *Steel and Pye* [1997]. In addition, the progressive adjustment of the simulated basin hypsometries as sediment supply increases (see Figure 4) and the change in the temporal evolution patterns of the scaling relationship between Ω and P translating a gradient from channel scouring to channel infilling under higher accretional activity (see Figure 8) constitute quantitative observations arguing that the synthetic tidal networks age faster under marsh accretional

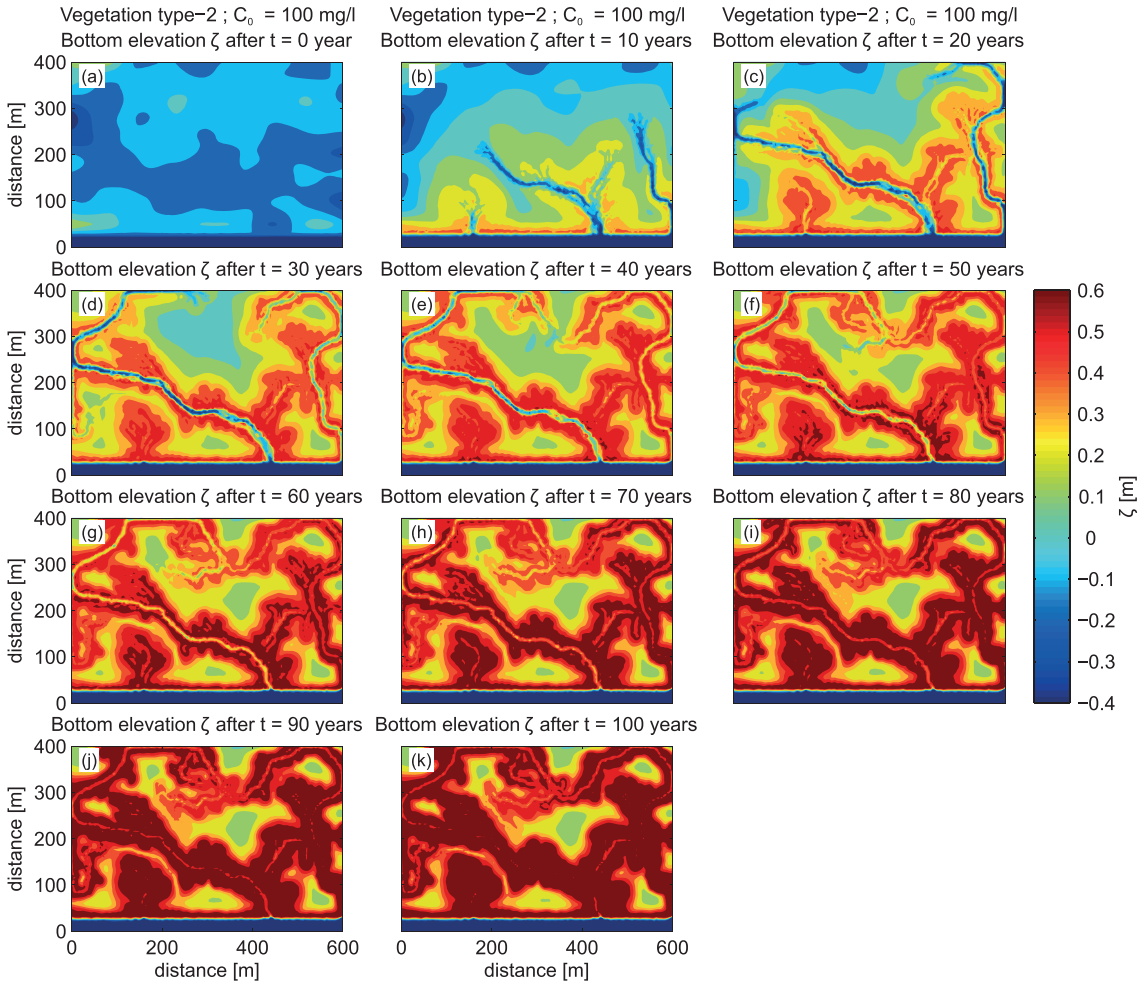

Figure 12. Long-term evolution (i.e., 100 years) of the marsh topography forced by a C_0 = 100 mg/L and vegetation type 2 scenario (corresponding to Figure 3l) computed with the continuous formulation (Figure 1d).

context. The increase in drainage density, hence network complexity, with increasing SSC (see Figure 9) also supports this observation. We deem this to be a critical feature of tidal network dynamics that previous studies missed to address.

This accelerated morphological evolution of tidal networks with higher sediment supply is ascribed to the more pronounced aggradation and progradation of the marsh platform which constrict faster and to a greater extent tidal channels. In response, channels rapidly extend and elaborate notably through elongation or first-order tributary initiation in order to accommodate the tidal prism that passes through them, leading eventually to high degree of channel complexity. Similarly, the critical point whereby channels start depicting signs of senescence due to the progressively reduced tidal prism and tidal velocities in the channel as the marsh platform reaches high elevations within the tidal frame occurs faster.

Evidences for accelerated tidal network development under high accretional activity can be also deduced from Figure 5. Indeed, the described morphological evolution of the simulated tidal landscape can be juxtaposed to the evolution of the tidal channels. Therefore, the first period of high morphological change, which appears earlier and in greater extent as sediment supply increases, is manifested by the channel initiation process, triggering the whole morphodynamic system that is far from its equilibrium configuration. Then, the slow and gradual decrease in the system morphological evolution is associated with the progressive elaboration followed by the senescence of the channels, being particularly marked in simulations characterized by high sediment supply, while the system approaches a morphological stable state.

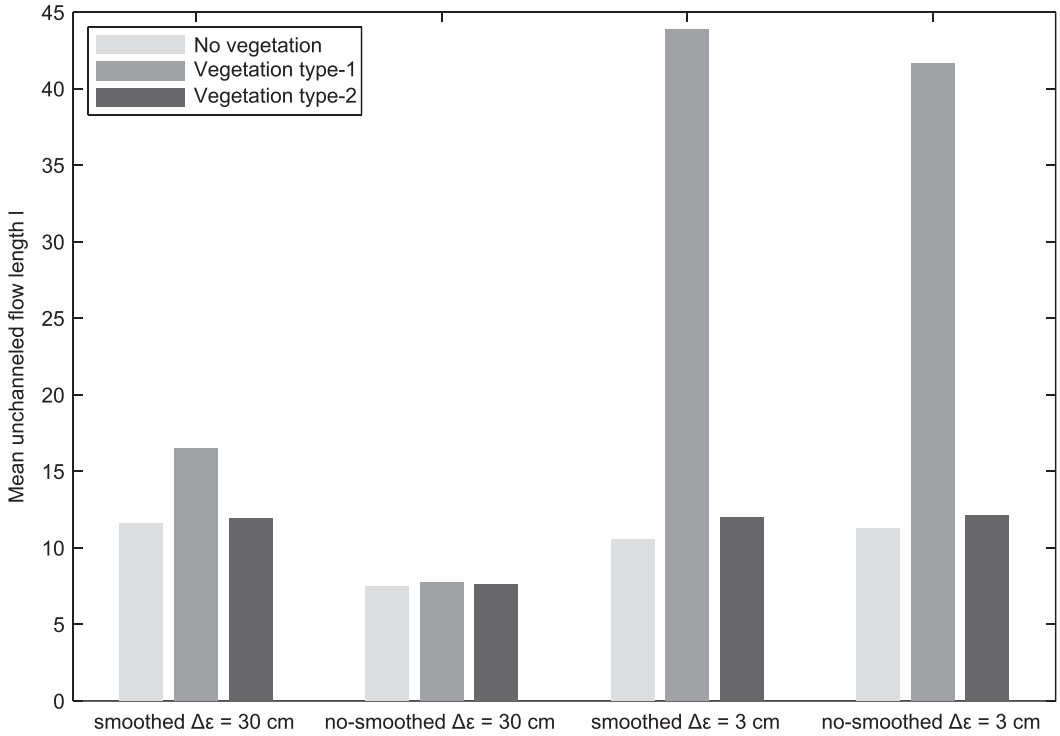

Figure 13. Mean unchanneled flow lengths *l* for the simulated morphologies from Figure 10. The drainage density is defined as the corresponding inverse value.

The initial basin topography reveals also to play a crucial role in determining tidal network evolution. The characteristics of the planform morphologies from Figure 10 have notably indicated that network complexity seems to be linked to the heterogeneity of topographic surface. As the role of local heterogeneities increases (by increasing the amplitude of local perturbations of the topography), the complexity of the channel network increases. To quantify this relationship, Figure 13 displays the values of the mean unchanneled flow lengths *l* for the simulated morphologies from Figure 10. Results show that the lowest values of the mean unchanneled flow lengths *l* occur for tidal networks formed over initial highly perturbed tidal basins. Accordingly, their corresponding high drainage densities evoke tidal networks characterized by an intricate morphology consisting of elongated and sinuous tidal channels and with the appearance of lower order creeks (see Figures 10d – 10f). This observation may be explained by the fact that the local topographic bumps and troughs composing the initial mudflat tend to guide the course of the forming tidal channels resulting therefore in a complex and elaborated tidal network as the topographic surface becomes rougher. Our results, obtained by solving the complete hydrodynamic and sediment transport equations, are in analogy with those obtained by *D'Alpaos et al.* [2005], on the basis of a simplified version of the shallow water equations and a conceptualized model of network growth. Those authors, in fact, observed that channel complexity and branching features increased with the effects of local heterogeneous geomorphological constraints, capable to affect network development.

In truth, these results support the concept of inheritance of the major tidal channel features from the morphological characteristics of the underlying mudflat and confirms the legacy left by the initial conditions, in this case the topography, on landscape evolution, as put forward also in previous studies [e.g., *Allen*, 2000; *Friedrichs and Perry*, 2001; *Marani et al.*, 2003; *Fagherazzi et al.*, 2004; *Perron and Fagherazzi*, 2012; *Stefanon et al.*, 2012].

As for the role of the vegetation in tidal channel morphodynamics, its impact on network development highly depends on its vertical biomass distribution within the tidal frame. Figures 3 and 10 show that the vegetation type 1 (monospecific) scenario, characterized by a high biomass productivity at the lower positions in the tidal frame (alluding therefore to its presence in the initial mudflat), may influence channel initiation processes. This

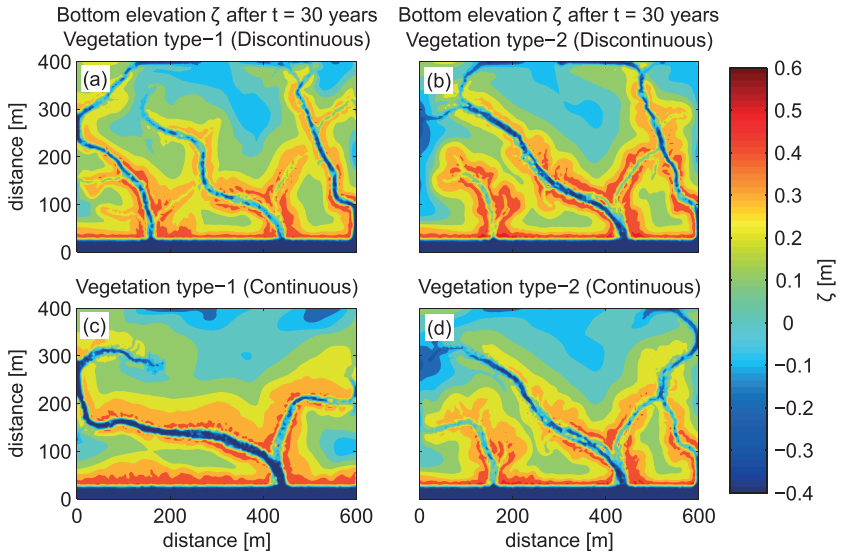

Figure 14. Simulated marsh morphologies after 30 years under a sediment supply C_0 = 50 mg/L and according to the two vegetation type scenarios (a and c) type 1 and (b and d) type 2, each being computed using the discontinuous formulations (9)–(10) (Figures 14a and 14b) and the continuous formulation (8) (Figures 14c and 14d).

is particularly illustrated looking at the high discrepancies in channel morphologies between the simulations with vegetation type 1 scenario and those without vegetation colonization.

On the other hand, the vegetation type 2 (multiple species) scenario characterized by a high biomass productivity at the upper positions in the tidal frame, alluding therefore to its absence in the initial mudflat, may only contribute to channel elaboration processes, such as channel lengthening and channel lateral migration as the network imprinting already arose prior to vegetation colonization. As a matter of fact, only local differences exist which concern shifts in channel course locations and degree of extension, while channel mouth location remains identical, between the simulations with vegetation type 2 scenario and those without vegetation colonization.

Therefore, depending on its presence or absence during the short time span in which channel initiation occurs, vegetation may be seen either as an erosive or a stabilizing agent for tidal channel development, as documented also by *Temmerman et al.* [2007] and *Schwarz et al.* [2014].

Up to this point, the different simulation sets have addressed vegetation biomass growth using the continuous formulation (see equation (8)). Owing to the current challenge in transcribing mathematically vegetation dynamics, one may question the sensitivity of the present mathematical expression in reproducing accurately this biotic process. Figure 14 displays final planform morphologies for the two different marsh ecological scenarios, keeping a constant suspended sediment concentration value $C_0 = 50$ mg/L and focusing on the comparison between the two biomass formulations from a mathematical point of view (continuous and discontinuous). Results show a diversity of morphologies even for the same ecological scenario. Particularly, substantial discrepancies in channel density and location occur between the two mathematical functions simulating marsh colonized by vegetation type 1 (Figures 14a and 14c) because, as discussed above, vegetation in this scenario immediately intervenes in the imprinting of the channel network.

Such differences indicate that the landscape morphodynamic evolution appears to be highly sensitive to the way the biomass growth is formulated. Consequently, real care should be dedicated when parameterizing such a dynamical process.

5. Conclusions

We performed a series of numerical experiments aiming to investigate tidal channel initiation and further elaboration with increasing marsh accretional activity. In such environmental condition, the analysis has shown that the development of tidal networks becomes the product of erosional and depositional processes acting at different stages within the ontogeny of tidal networks: channel origination stems from bottom

incision in regions where initial local depressions occur, while channel elaboration mostly results from differential deposition. This critical aspect is quantitatively addressed here for the first time. The further evolutionary stages, such as channel reduction, proceed from the continuous aggradation and progradation of the marsh platform leading to channel narrowing and, eventually, channel segmentation and closure.

Tidal network development is also accelerated in sedimentary contexts characterized by high sediment supply. Although such an effect seems to be trivial when looking at the marsh morphological evolution, as marshes typically age while building up along the tidal frame, transposing such a concept to the tidal network landform appears to be rather counterintuitive as the majority of conceptual and mathematical models assume tidal channel development as mainly resulting from erosional activity. Such an observation emphasizes the high magnitude, hence prevalence, of the depositional processes in shaping the tidal network. Moreover, putting this concept in line with the exposed legacy of the initial topography on tidal channel morphological features, the overall results eventually highlight the tight coupling of the tidal network with the tidal flat and salt marsh landforms onto which it develop and the necessity to adopt a holistic approach by considering the tidal wetland as a whole reference system when investigating tidal network morphodynamics, particularly in high sediment supply settings.

Lastly, the outcomes have also confirmed the high contribution of the vegetation in driving tidal channel morphological evolution and therefore the relevance of acknowledging it as a real control in tidal network morphodynamics, justifying once again the use of a holistic approach. Nevertheless, results have shown a sensitivity of the dynamic response of the system to the parameterization of the vegetation growth. This calls for the necessity to ensure an accurate definition of such a process in a mathematical fashion, and in view of the current challenge in doing so, future research should particularly focus on this issue.

Acknowledgments

The presented modeling framework is developed on the basis of a research-based numerical model which is not open access presently and therefore cannot be shared publically. This work has been carried out within the SMART Joint Doctorate (Science for MAnagement of Rivers and their Tidal systems) funded with the support of the Erasmus Mundus programme of the European Union and the 2013 University of Padova project: "Combined use of remote sensing and in situ measurements for the calibration of transport and diffusion models in shallow coastal lagoons" (CPDA133253/13). We thank the CARIPARO project titled "Reading signatures of the past to predict the future: 1000 years of stratigraphic record as a key for the future of the Venice Lagoon" for funding contribution. We warmly thank Alessandra Crosato for her expertise and critical judgment on the modeling framework that have represented definite benefits for the good completion of this research work. We also gratefully recognize the contributions of the Editor and two anonymous reviewers that allowed us to refine the manuscript effectively.

References

Allen, J. R. L. (2000), Morphodynamics of Holocene salt marshes: A review sketch from the Atlantic and Southern North Sea coasts of Europe, *Quat. Sci. Rev.*, *19*(12), 1155–1231.

Amos, C., A. Bergamasco, G. Umgiesser, S. Cappucci, D. Cloutier, L. DeNat, M. Flindt, M. Bonardi, and S. Cristante (2004), The stability of tidal flats in Venice Lagoon—The results of in-situ measurements using two benthic, annular flumes, *J. Mar. Syst.*, *51*(1), 211–241.

Barbier, E. B., S. D. Hacker, C. Kennedy, E. W. Koch, A. C. Stier, and B. R. Silliman (2011), The value of estuarine and coastal ecosystem services, *Ecol. Monogr.*, *81*(2), 169–193.

Beeftink, W. (1966), Vegetation and habitat of the salt marshes and beach plains in the south-western part of the Netherlands, *Wentia*, *15*, 83–108.

Bouma, T., M. Friedrichs, B. Van Wesenbeeck, S. Temmerman, G. Graf, and P. Herman (2009), Density-dependent linkage of scale-dependent feedbacks: A flume study on the intertidal macrophyte Spartina anglica, *Oikos*, *118*(2), 260–268.

Carniello, L., A. Defina, S. Fagherazzi, and A. D'alpaos (2005), A combined wind wave-tidal model for the Venice Lagoon, Italy, *J. Geophys. Res.*, *110*, F04007, doi:10.1029/2004JF000232.

Carniello, L., A. D'Alpaos, and A. Defina (2011), Modeling wind waves and tidal flows in shallow micro-tidal basins, *Estuarine Coastal Shelf Sci.*, *92*(2), 263–276.

Carniello, L., A. Defina, and L. D'Alpaos (2012), Modeling sand-mud transport induced by tidal currents and wind waves in shallow microtidal basins: Application to the Venice Lagoon (Italy), *Estuarine Coastal Shelf Sci.*, *102*, 105–115.

Carniello, L., S. Silvestri, M. Marani, A. D'Alpaos, V. Volpe, and A. Defina (2014), Sediment dynamics in shallow tidal basins: In situ observations, satellite retrievals, and numerical modeling in the Venice Lagoon, *J. Geophys. Res. Earth Surf.*, *119*, 802–815, doi:10.1002/2013JF003015.

Chow, V. T. (1959), *Open-Channel Hydraulics*, McGraw-Hill, New York.

Christiansen, T., P. Wiberg, and T. Milligan (2000), Flow and sediment transport on a tidal salt marsh surface, *Estuarine Coastal Shelf Sci.*, *50*(3), 315–331.

Coco, G., Z. Zhou, B. van Maanen, M. Olabarrieta, R. Tinoco, and I. Townend (2013), Morphodynamics of tidal networks: Advances and challenges, *Mar. Geol.*, *346*, 1–16.

D'Alpaos, A., S. Lanzoni, M. Marani, S. Fagherazzi, and A. Rinaldo (2005), Tidal network ontogeny: Channel initiation and early development, *J. Geophys. Res.*, *110*, F02001, doi:10.1029/2004JF000182.

D'Alpaos, A., S. Lanzoni, S. M. Mudd, and S. Fagherazzi (2006), Modeling the influence of hydroperiod and vegetation on the cross-sectional formation of tidal channels, *Estuarine Coastal Shelf Sci.*, *69*(3), 311–324.

D'Alpaos, A., S. Lanzoni, M. Marani, and A. Rinaldo (2007), Landscape evolution in tidal embayments: Modeling the interplay of erosion, sedimentation, and vegetation dynamics, *J. Geophys. Res.*, *112*, F01008, doi:10.1029/2006JF000537.

D'Alpaos, A., S. Lanzoni, M. Marani, and A. Rinaldo (2010), On the tidal prism-channel area relations, *J. Geophys. Res.*, *115*, F01003, doi:10.1029/2008JF001243.

De Swart, H., and J. Zimmerman (2009), Morphodynamics of tidal inlet systems, *Ann. Rev. Fluid Mech.*, *41*, 203–229.

Defina, A. (2000), Two-dimensional shallow flow equations for partially dry areas, *Water Resour. Res.*, *36*(11), 3251–3264.

Fagherazzi, S., and D. J. Furbish (2001), On the shape and widening of salt marsh creeks, *J. Geophys. Res.*, *106*(C1), 991–1003.

Fagherazzi, S., and I. Overeem (2007), Models of deltaic and inner continental shelf landform evolution, *Annu. Rev. Earth Planet. Sci.*, *35*, 685–715.

Fagherazzi, S., E. J. Gabet, and D. J. Furbish (2004), The effect of bidirectional flow on tidal channel planforms, *Earth Surf. Processes Landforms*, *29*(3), 295–309.

Fagherazzi, S., et al. (2012), Numerical models of salt marsh evolution: Ecological, geomorphic, and climatic factors, *Rev. Geophys.*, *50*, RG1002, doi:10.1029/2011RG000359.

Feola, A., E. Belluco, A. D'Alpaos, S. Lanzoni, M. Marani, and A. Rinaldo (2005), A geomorphic study of lagoonal landforms, *Water Resour. Res.*, *41*, W06019, doi:10.1029/2004WR003811.
French, J. R., and D. Stoddart (1992), Hydrodynamics of salt marsh creek systems: Implications for marsh morphological development and material exchange, *Earth Surf. Processes Landforms*, *17*(3), 235–252.
Frey, R. W., and P. B. Basan (1978), Coastal salt marshes, in *Coastal Sedimentary Environments*, edited by R. A. Davis Jr., pp. 101–169, Springer, New York.
Friedrichs, C. T., and J. E. Perry (2001), Tidal salt marsh morphodynamics: A synthesis, *J. Coastal Res.*, *27*, 7–37.
Gibbs, R. J. (1985), Estuarine flocs: Their size, settling velocity and density, *J. Geophys. Res.*, *90*(C2), 3249–3251.
Glock, W. S. (1931), The development of drainage systems: A synoptic view, *Geog. Rev.*, *21*, 475–482.
Hood, W. G. (2006), A conceptual model of depositional, rather than erosional, tidal channel development in the rapidly prograding Skagit River Delta (Washington, USA), *Earth Surf. Processes Landforms*, *31*(14), 1824–1838.
Hood, W. G. (2010), Tidal channel meander formation by depositional rather than erosional processes: Examples from the prograding Skagit River Delta (Washington, USA), *Earth Surf. Processes Landforms*, *35*(3), 319–330.
Hughes, Z. J. (2012), Tidal channels on tidal flats and marshes, in *Principles of Tidal Sedimentology*, edited by R. A. Davis Jr. and R. W. Dalrymple, pp. 269–300, Springer, Netherlands.
Hughes, Z. J., D. M. FitzGerald, C. A. Wilson, S. C. Pennings, K. Wieski, and A. Mahadevan (2009), Rapid headward erosion of marsh creeks in response to relative sea level rise, *Geophys. Res. Lett.*, *36*, L03602, doi:10.1029/2008GL036000.
Jarrett, J. T. (1976), Tidal prism-inlet area relationships, *Tech. Rep.*, U.S. Army Coastal Eng. Res. Cent., Fort Belviour, Va.
Jones, C. G., J. H. Lawton, and M. Shachak (1994), Organisms as ecosystem engineers, *Oikos*, *69*(3), 373–386.
Kirwan, M. L., and A. B. Murray (2007), A coupled geomorphic and ecological model of tidal marsh evolution, *Proc. Natl. Acad. Sci.*, *104*(15), 6118–6122.
Krone, R. B. (1962), Flume studies of the transport of sediment in estuarial shoaling processes, *Tech. Rep., Hydr.*, Eng. Lab., Univ. of Berkely, USA.
Leonard, L. A., and A. L. Croft (2006), The effect of standing biomass on flow velocity and turbulence in Spartina alterniflora canopies, *Estuarine Coastal Shelf Sci.*, *69*(3), 325–336.
Leonard, L. A., and M. E. Luther (1995), Flow hydrodynamics in tidal marsh canopies, *Limnol. Oceanogr.*, *40*(8), 1474–1484.
Marani, M., E. Belluco, A. D'Alpaos, A. Defina, S. Lanzoni, and A. Rinaldo (2003), On the drainage density of tidal networks, *Water Resour. Res.*, *39*(2), 1040, doi:10.1029/2001WR001051.
Marani, M., S. Lanzoni, S. Silvestri, and A. Rinaldo (2004), Tidal landforms, patterns of halophytic vegetation and the fate of the lagoon of Venice, *J. Mar. Syst.*, *51*(1), 191–210.
Marani, M., A. D'Alpaos, S. Lanzoni, L. Carniello, and A. Rinaldo (2007), Biologically-controlled multiple equilibria of tidal landforms and the fate of the Venice Lagoon, *Geophys. Res. Lett.*, *34*, L11402, doi:10.1029/2007GL030178.
Marani, M., A. D'Alpaos, S. Lanzoni, L. Carniello, and A. Rinaldo (2010), The importance of being coupled: Stable states and catastrophic shifts in tidal biomorphodynamics, *J. Geophys. Res.*, *115*, F04004, doi:10.1029/2009JF001600.
Marani, M., C. Da Lio, and A. D'Alpaos (2013), Vegetation engineers marsh morphology through multiple competing stable states, *Proc. Natl. Acad. Sci.*, *110*(9), 3259–3263.
Marciano, R., Z. B. Wang, A. Hibma, H. J. de Vriend, and A. Defina (2005), Modeling of channel patterns in short tidal basins, *J. Geophys. Res.*, *110*, F01001, doi:10.1029/2003JF000092.
Morris, J. T., and B. Haskin (1990), A 5-yr record of aerial primary production and stand characteristics of Spartina alterniflora, *Ecology*, *71*(6), 2209–2217.
Morris, J. T., P. Sundareshwar, C. T. Nietch, B. Kjerfve, and D. Cahoon (2002), Responses of coastal wetlands to rising sea level, *Ecology*, *83*(10), 2869–2877.
Morris, J. T., D. Porter, M. Neet, P. A. Noble, L. Schmidt, L. A. Lapine, and J. R. Jensen (2005), Integrating LIDAR elevation data, multi-spectral imagery and neural network modelling for marsh characterization, *Int. J. Remote Sens.*, *26*(23), 5221–5234.
Mudd, S. M., S. Fagherazzi, J. T. Morris, and D. J. Furbish (2004), Flow, sedimentation, and biomass production on a vegetated salt marsh in South Carolina: Toward a predictive model of marsh morphologic and ecologic evolution, *Coastal Estuarine Stud.*, *59*, 165–188.
Mudd, S. M., A. D'Alpaos, and J. T. Morris (2010), How does vegetation affect sedimentation on tidal marshes? Investigating particle capture and hydrodynamic controls on biologically mediated sedimentation, *J. Geophys. Res.*, *115*, F03029, doi:10.1029/2009JF001566.
O'Brien, M. P. (1969), Equilibrium flow areas of tidal inlets on sandy coasts, *Coastal Eng. Proc.*, *1*(10), 42–52.
Palmer, M. R., H. M. Nepf, T. J. Pettersson, and J. D. Ackerman (2004), Observations of particle capture on a cylindrical collector: Implications for particle accumulation and removal in aquatic systems, *Limnol. Oceanogr.*, *49*(1), 76–85.
Perillo, G. M. (2009), Tidal courses: Classification, origin and functionality, in *Coastal Wetlands: An Integrated Ecosystem Approach*, edited by G. M. Perillo et al., pp. 185–210, Elsevier, Amsterdam.
Perillo, G. M., and O. O. Iribarne (2003a), New mechanisms studied for creek formation in tidal flats: From crabs to tidal channels, *Eos Trans. AGU*, *84*(1), 1–5.
Perillo, G. M., and O. O. Iribarne (2003b), Processes of tidal channel development in salt and freshwater marshes, *Earth Surf. Processes Landforms*, *28*(13), 1473–1482.
Perillo, G. M., M. D. Ripley, M. C. Piccolo, and K. R. Dyer (1996), The formation of tidal creeks in a salt marsh: New evidence from the Loyola Bay Salt Marsh, Rio Gallegos Estuary, Argentina, *Mangroves Salt Marshes*, *1*(1), 37–46.
Perron, J., and S. Fagherazzi (2012), The legacy of initial conditions in landscape evolution, *Earth Surf. Processes Landforms*, *37*(1), 52–63.
Pritchard, D., and A. Hogg (2003), Cross-shore sediment transport and the equilibrium morphology of mudflats under tidal currents, *J. Geophys. Res.*, *108*(C10), 3313, doi:10.1029/2002JC001570.
Randerson, P. (1979), A simulation model of salt-marsh development and plant ecology, in *Estuarine and Coastal Land Reclamation and Water Storage*, edited by B. Knights and A. J. Phillips, pp. 48–67, Saxon House, Farnborough, England.
Redfield, A. C. (1972), Development of a New England salt marsh, *Ecol. Monogr.*, *42*, 201–237.
Rinaldo, A., S. Fagherazzi, S. Lanzoni, M. Marani, and W. E. Dietrich (1999), Tidal networks: 2. Watershed delineation and comparative network morphology, *Water Resour. Res.*, *35*(12), 3905–3917.
Roelvink, J. (2006), Coastal morphodynamic evolution techniques, *Coastal Eng.*, *53*(2), 277–287.
Schwarz, C., Q. Ye, D. Wal, L. Zhang, T. Bouma, T. Ysebaert, and P. Herman (2014), Impacts of salt marsh plants on tidal channel initiation and inheritance, *J. Geophys. Res. Earth Surf.*, *119*, 385–400, doi:10.1002/2013JF002900.
Silvestri, S., A. Defina, and M. Marani (2005), Tidal regime, salinity and salt marsh plant zonation, *Estuarine Coastal Shelf Sci.*, *62*(1), 119–130.
Steel, T. J., and K. Pye (1997), The development of salt marsh tidal creek networks: Evidence from the UK. paper presented at Canadian Coastal Conference, Can. Coastal Sci. and Eng. Assoc., Guelph, Ontario, vol. 1, pp. 267–280.

Stefanon, L., L. Carniello, A. D'Alpaos, and S. Lanzoni (2010), Experimental analysis of tidal network growth and development, *Cont. Shelf Res.*, *30*(8), 950–962.
Stefanon, L., L. Carniello, A. D'Alpaos, and A. Rinaldo (2012), Signatures of sea level changes on tidal geomorphology: Experiments on network incision and retreat, *Geophys. Res. Lett.*, *39*, L12402, doi:10.1029/2012GL051953.
Temmerman, S., T. Bouma, G. Govers, and D. Lauwaet (2005), Flow paths of water and sediment in a tidal marsh: Relations with marsh developmental stage and tidal inundation height, *Estuaries*, *28*, 338–352.
Temmerman, S., T. Bouma, J. Van de Koppel, D. Van der Wal, M. De Vries, and P. Herman (2007), Vegetation causes channel erosion in a tidal landscape, *Geology*, *35*(7), 631–634.
Toffolon, M., and S. Lanzoni (2010), Morphological equilibrium of short channels dissecting the tidal flats of coastal lagoons, *J. Geophys. Res.*, *115*, F04036, doi:10.1029/2010JF001673.
Torres, R., and R. Styles (2007), Effects of topographic structure on salt marsh currents, *J. Geophys. Res.*, *112*, F02023, doi:10.1029/2006JF000508.
Van Maanen, B., G. Coco, and K. Bryan (2013a), Modelling the effects of tidal range and initial bathymetry on the morphological evolution of tidal embayments, *Geomorphology*, *191*, 23–34.
Van Maanen, B., G. Coco, K. Bryan, and C. Friedrichs (2013b), Modeling the morphodynamic response of tidal embayments to sea-level rise, *Ocean Dyn.*, *63*(11–12), 1249–1262.
Van Rijn, L. C. (1984), Sediment transport. Part I: Bed load transport, *J. Hydraul. Eng.*, *110*(10), 1431–1456.
Wang, C., M. Menenti, M.-P. Stoll, A. Feola, E. Belluco, and M. Marani (2009), Separation of ground and low vegetation signatures in lidar measurements of salt-marsh environments, *IEEE Trans. Geosci. Remote Sens.*, *47*(7), 2014–2023.
Yapp, R., D. Johns, and O. Jones (1917), The salt marshes of the Dovey Estuary, *J. Ecol.*, *5*, 65–103.